POLITECNICO DI TORINO

MASTER'S DEGREE IN MECHANICAL ENGINEERING

MASTER'S THESIS ENTITLED

Dynamic wake modelling and simulation for offshore wind turbines

Supervisor:
Dr. Fabio Carapellese

Co-Supervisors:
Ing. Davide Issoglio
Prof. Giovanni Bracco

Candidate:
Mongelli Francesco

Academic year 2024-2025

ABSTRACT

Achieving net-zero carbon emissions requires continuous improvements in renewable energy conversion systems. This thesis focuses on such improvement, in the context of offshore wind turbines.

When it comes to wind farms, it is essential to understand how the different turbines interact with each other through their wakes. A better understanding of these phenomena can lead to more efficient controlling strategies, maximizing power extraction.

This work presents an approach to wake modelling which differs from the common ones implemented in current simulation tools. The proposed model simulates wakes dynamically, allowing it to account for changing wind conditions, both in speed and direction, and visualize wake propagation over time.

The model has been implemented in the tool MOST, a Matlab/Simulink environment for high-fidelity simulation of wind turbines.

The case study consists of two turbines, one upstream and one downstream. It is analysed how the behaviour of the downstream turbine changes when the wake model presented is implemented. Comparing the power output and the different dynamic behaviours can justify the use of dynamic wake models like the one presented.

ACKNOWLEDGEMENTS

I would like to express my gratitude to Prof. Giovanni Bracco for giving me the opportunity to carry out my Master's thesis at the MOREnergy Lab.
I am also sincerely thankful to Ing. Davide Issoglio and Dr. Fabio Carapellese for their support, kindness, and availability throughout the entire development of my thesis. Their guidance was always effective, and I appreciated knowing I could rely on their help for any need.

Table of contents

List of Figures

List of Acronyms

ABL	Atmospheric Boundary Layer
BEM	Beam Element Momentum
CFD	Computational Fluid Dynamics
CVP	Counter rotating Vortex Pair
DNS	Direct Numerical Simulation
DS	Downstream
DWT	Downstream Wind Turbine
FLORIDyn	FLOw Redirection and Induction Dynamics
FLORIS	FLOw Redirection and Induction in Steady State
LES	Large Eddy Simulation
MOST	MATLAB OFWT Simulation Tool
NREL	National Renewable Energy Laboratory
OFWT	Offshore Floating Wind Turbine
OP	Observation Points
RANS	Reynolds Averaged Navier-Stokes equations
ROSCO	Reference Open-Source COntroller
SOWFA	Simulator fOr Wind Farm Applications
UWT	Upstream Wind Turbine
WEC-Sim	Wave Energy Converter SIMulator

List of Symbols

δ	Wake deflection in the Gaussian model
σ_y	Wake width along the y axis
σ_z	Wake width along the z axis
f_x	Aerodynamic force along the x axis
f_y	Aerodynamic force along the y axis
a_{ax}	Axial induction factor
γ	Yaw angle
A	Frontal area of the rotor disk
$\Delta\bar{u}$	Velocity deficit in streamwise direction
C_T	Coefficient of thrust
C_P	Coefficient of Power
α	Skew angle in the Jimenez deflection model
θ	Skew angle in the Gaussian model
θ_c	Skew angle of the wake centre
δ_0	Wake deflection at the far wake onset
ϑ_{c_0}	Skew angle of the wake centre at the far wake onset
r	Reduction factor in FLORIDyn
$w_{y,pc}$	Potential core width in y direction
$w_{z,pc}$	Potential core width in z direction
$y_{1,\mathrm{OP}}$	OP's y coordinate in the wake coordinate system
$z_{1,\mathrm{OP}}$	OP's z coordinate in the wake coordinate system
$\mathrm{R}_{01}(\varphi_{0,\mathrm{OP}})$	Rotational matrix between wake and global coordinate FLORIDyn systems

v_0	Velocity just behind the rotor in Jensen deficit model
u	Free-stream velocity in Jensen deficit model
v	velocity within the wake at a given downstream coordinate x in the Jensen deficit model
α	entrainment constant in the Jensen deficit model
$m_{e,q}$	Wake expansion parameter in the multizone model
k_e	Wake expansion parameter in the multizone model
c	Wake decay coefficient in the multizone model
U_0	average freestream velocity at disk centre position in the Jimenez deflection model
ρ	Air density
D	Turbine diameter
β	Coefficient related to wake growth in the Jimenez model

Alla mia famiglia,
Ai miei amici,
A me stesso.

INTRODUCTION

The energy challenge we are currently facing is highly demanding and calls for continuous improvements in the energy sources at our disposal. Renewable energies represent a valid and sustainable option to meet growing energy demands while minimizing the environmental impact, particularly in terms of pollutant emissions. To make this transition feasible, a continuous effort in research and development is essential in order to optimize the available technologies. Among the most promising of these technologies are wind turbines, capable of converting the kinetic energy of wind into mechanical rotational energy and subsequently into electrical power. In particular, offshore wind turbines have gained significant traction in recent years, owing to several key advantages:

- Higher and more consistent wind speeds over open water compared to onshore sites, which results in increased energy production.
- Reduced visual and acoustic impact, making them more acceptable to the public and less intrusive to populated areas.
- Availability of larger installation areas, which allows for the deployment of large-scale wind farms without the spatial constraints typically found on land.

Despite these advantages, there remain many aspects that can be optimized. One critical aspect, and the specific focus of this thesis, is the mutual interaction between turbines within the same wind farm. This interaction manifests through the formation of wakes: regions of reduced wind velocity and increased turbulence downstream of a functioning turbine. A detailed characterization of the wake phenomena will be provided in Chapter 2. In a wind farm setting, turbines positioned downstream process a flow that has already been altered by upstream turbines, resulting in reduced power generation. It is therefore crucial to understand and accurately predict wake behaviour. A deeper understanding of wakes enables improved wind farm layout design and more effective control strategies for turbine operation.

In this context, the primary objective of this thesis is to implement a wake prediction model within MOST (Matlab OFWT Simulation Tool), a well-established tool for simulating offshore floating wind turbines (OFWTs). This implementation aims to enhance the modelling capabilities of MOST by integrating dynamic wake modelling functionality. In particular, Chapter 1 introduces MOST and outlines the key areas where modifications will be implemented. Chapter 2 presents a comprehensive review of the current state of the art in wake modelling, covering both steady-state and dynamic models, and explains the reasons behind

selecting FLORIDyn, a dynamic wake model, for implementation. Chapter 3 provides a detailed description of FLORIDyn, facilitating a clearer understanding of the implementation phase. Chapter 4 describes the actual process of integrating FLORIDyn into the MOST framework. Chapter 5 presents and discusses the results obtained from simulation campaigns carried out to test the coupling between MOST and FLORIDyn, followed by conclusions outlining the current limitations of the implementation and suggestions for further improvement.

CHAPTER 1. MODELLING FRAMEWORK – MOST

1.1 Introduction on MOST

MOST, Matlab OFWT Simulation Tool, is a simulation tool developed by MOREnergy Lab for the planning and design phase of offshore floating wind turbines [1]. It includes all the components of an offshore wind turbine (floating platform and hydrodynamics, wind turbine and aerodynamics, electric generator and its control law) and operates within the WEC-Sim environment, an open-source MATLAB/SIMULINK-based software for simulating wave energy converters. Compared to existing simulation tools, such as OpenFAST [2] (a state-of-the-art open-source software developed by the National Renewable Energy Laboratory (NREL) for offshore wind turbines), MOST represents a more flexible and easy-access tool.

1.2 MOST structure

The core of the tool is the Simulink model in which all components interact and communicate with each other in a modular framework. The following image represents a scheme of the various components of MOST:

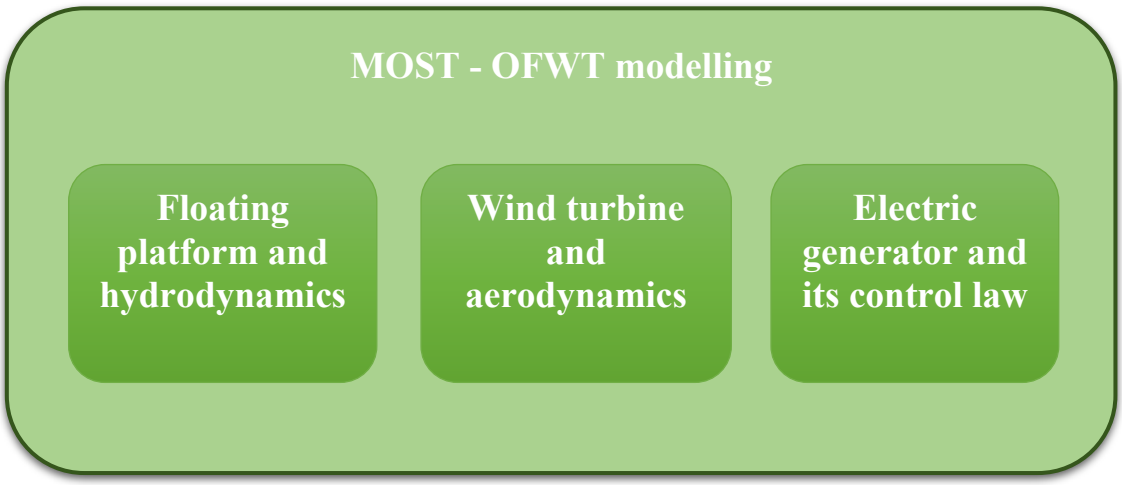

Figure 1 - schematic representation of the MOST framework

In the module "wind turbine and aerodynamics" each turbine component is defined in its geometry (for visualization purposes), mass and inertia. The components are linked together using models of joints, which account for the rotation between tower and nacelle and between nacelle and hub. Regarding the hydrodynamics, all the necessary hydrostatic/hydrodynamic information must be provided as input to the simulation. The information is generated from the

results of an external BEM (Boundary Element Method) software with the BEMIO (Boundary Element Method Input/Output) functions of WEC-Sim. A more complete insight into MOST structure and functioning can be found on the official documentation [1]. The next paragraph focuses on how the wind input is generated and utilized in MOST. This will be useful to introduce the purpose of this thesis.

1.3 Aerodynamics in MOST

MOST is capable of generating both turbulent wind fields and non-turbulent wind fields. In the first case an external code is used, Turbsim, developed by NREL, and integrated within the MOST code. The user can specify some properties such as mean velocity and turbulence intensity. Regarding the second case, it is possible to define a uniform wind field and specify speed and direction over time. In both cases the resulting data structure consists of the wind speed at each instant and for each node of a spatial grid covering the rotor area. Once the wind signal is generated, it can be used to calculate the aerodynamical forces acting on the turbine. To do that the tool offers two ways, via lookup tables or by using the BEM (Beam Element Momentum) method. In this thesis the latter will be used. Once the aerodynamic forces acting on the turbine blades have been computed, these forces serve as the primary input for determining the dynamic response of the turbine.
The purpose of this thesis is to extend the modelling capabilities of MOST. More specifically, the objective is to implement a model that can simulate the generation and evolution of a wake downstream of the wind turbine, starting from parameters calculated from the simulation. Therefore, a good understanding of the various existing wake models is necessary, in order to choose the one that is more appropriate for the implementation. These considerations will be further developed and discussed in the following chapter.

CHAPTER 2. BACKGROUND

2.1 Wake

With the term *wake* we indicate the altered region downstream of an operating wind turbine. This region is the result of the extraction of wind energy by the turbine and is characterized by a reduced wind velocity and an increased turbulence intensity.

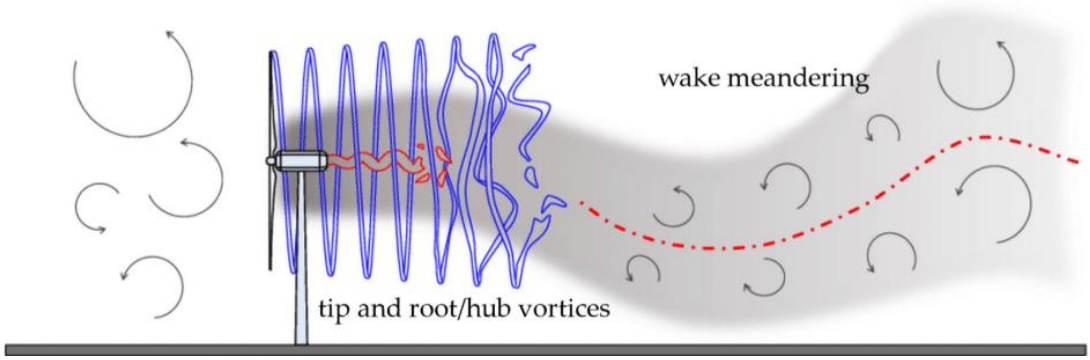

Figure 2 - schematic representation of the instantaneous wind field behind a turbine [3]. The wake is a complex phenomenon deriving from the combination of various effects. In this image the tip and root/hub vortices are depicted, and it is given a representation of the wake meandering effect, which is a low-frequency oscillation of the entire wake

Even though the wake of a wind turbine is a highly complex phenomenon, strongly influenced by the turbine's operational parameters (such as yaw misalignment, thrust coefficient *Ct*, and other factors) as well as the characteristics of the incoming wind, it is still possible to identify recurring patterns.

In particular, the wake evolution can be broadly divided into two regions:

1. Near-wake region: This is the area immediately downstream of the turbine (and extends 1 – 2 times the diameter downstream), where the flow is primarily governed by the turbine's rotor-induced velocity deficit and by mean velocities gradients. Turbulence levels are moderate.
2. Far-wake region: At greater distances downstream, the wake transitions into a fully turbulent free shear flow. In this region, the influence of the turbine's specific operational details diminishes, and the flow is dominated by turbulent mixing and diffusion processes. As it evolves, the flow gradually recovers its original free wind velocity.

Alongside with the evolution of the wake downstream, the flow is also altered in the cross-sectional area of the wake. In fact, the wake gradually expands and deflects. The deflection is primarily due to yaw misalignment. Another effect that alters the wake on the altitude direction is the vertical wind shear.

2.2 Wake modelling

As seen in the previous paragraph, wakes are a complex phenomenon that takes into account many variables. When it comes to model such phenomena, several different approaches have been pursued in literature. These approaches vary widely in terms of complexity and underlying assumptions, ranging from simplified analytical models (which are called low-fidelity) to high-fidelity numerical simulations, including Reynolds-Averaged Navier-Stokes (RANS) and Large Eddy Simulations (LES).

This thesis will focus specifically on low-fidelity approaches. These methods are particularly useful for applications where computational efficiency is a priority, such as preliminary design, control strategy development, or large-scale wind farm simulations.

Among the tools commonly used within this category there is OpenFAST [2], an open-source, modular wind turbine simulation framework developed by NREL, which allows for the aero-hydro-servo-elastic analysis of wind turbines using simplified physical models.

Apart from the specific tool utilized, a wake model is usually made up of four components:

1. Velocity deficit model
2. Wake deflection model
3. Turbulence model
4. Wake combination model

To better understand how a wake model works as a whole, a description of each of the mentioned components will be given.

2.3 Velocity deficit models

In the previous paragraphs it has been said that a wake is the altered region behind an operating wind turbine, characterized by reduced wind speed and increased turbulence. So, primarily, a wake model should mathematically represent the distribution of the velocity deficit spreading with the wake. Various formulations have been proposed in literature. In this section the approaches that will be presented are:

- Jensen model, in which the velocity is uniform in a section and recovers downstream
- Multizone model, in which the wake is divided in zones, each with its own evolution
- Gaussian model, in which the deficit derives from budget analysis of RANS equations

Having briefly introduced the models, now a more detailed description of each one of them will be presented.

2.3.1 Jensen Model

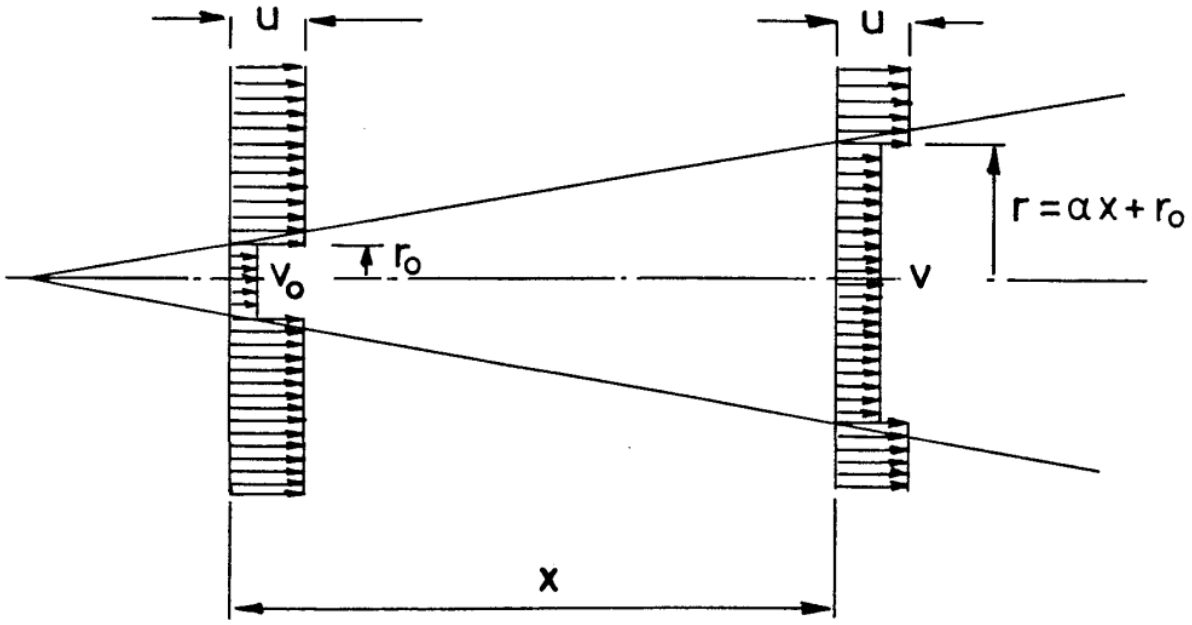

Figure 3 - schematic representation of the wake for the Jensen wake model [4]

The Jensen wake model [4] treats the wake as fully turbulent, neglecting the complex near wake contributions. This model is also referred to as "top-hat", because it assumes that the velocity within the wake does not vary along the spanwise direction. Additionally, it assumes that the free-stream velocity is fully recovered beyond the boundaries of the wake region of interest. Under these assumptions, the wake radius increase linearly with downstream distance, as can be seen in the Figure 3. By performing a momentum balance, the following equation is obtained:

$$\pi r_0^2 v_0 + \pi(r^2 - r_0^2)u = \pi r^2 v \tag{1}$$

Where:

- v_0 is the velocity just behind the rotor,
- u is the free-stream velocity,
- v is the velocity within the wake at a given downstream coordinate x

If a linear relationship is assumed between the wake radius and the downstream distance x, and if the velocity immediately behind the rotor is assumed to be one-third of the free-stream velocity, equation (*1*) can be solved for v, resulting in the following expression:

$$v = u\left[1 - \frac{2}{3}\left(\frac{r_0}{r_0 + \alpha x}\right)^2\right] \tag{2}$$

Where α is the entrainment constant. It has been stated that the model assumes a "top-hat" velocity deficit profile. However, this assumption does not accurately reflect the experimental data. To address this discrepancy, the author introduces the possibility to use a corrective function aimed at improving the model's agreement with experimental observations.

$$f(\theta) = \frac{1 + \cos(9\theta)}{2}; \qquad \theta \leqslant 20^{\circ}, \tag{3}$$

In the following image equation (*1*) is plotted using the value of 0.1 for α both with and without correction (*3*), against experimental data from Vermeulen et al. [5]:

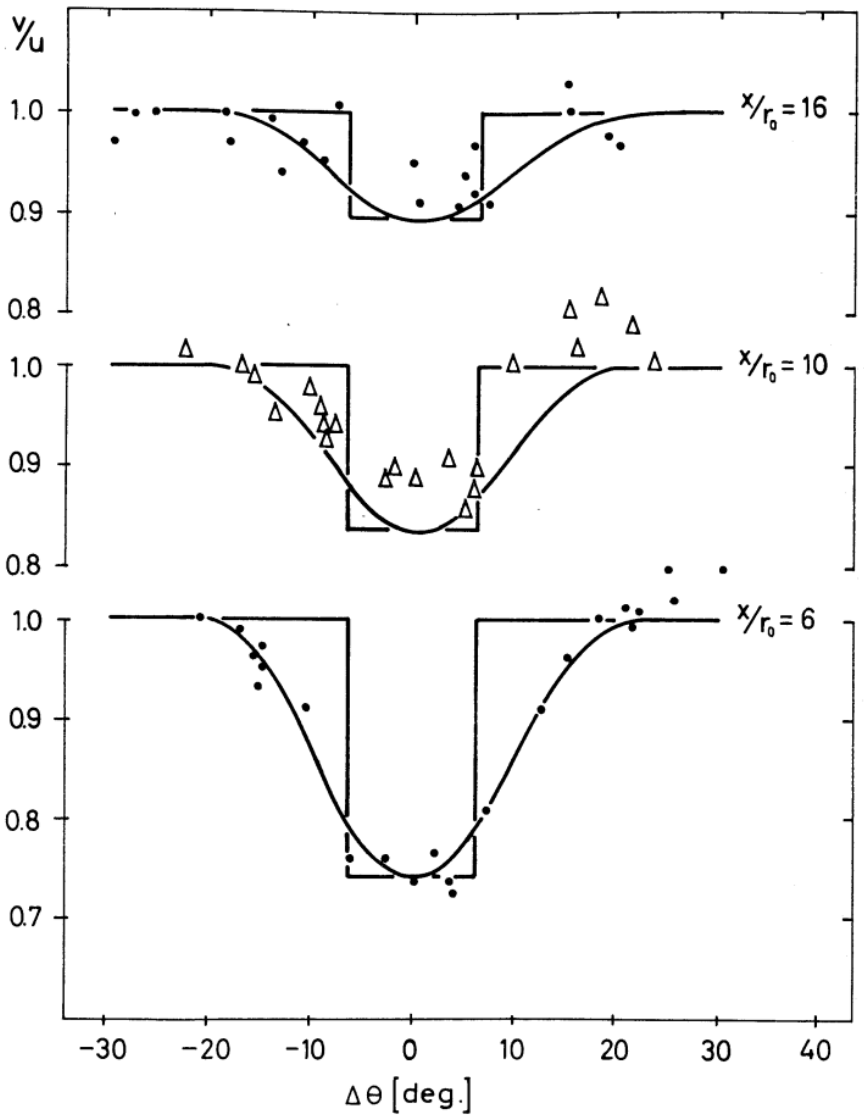

Figure 4 - experimental results averaged on a time span of 256 s (Vermeulen et al. [5]) are plotted with predictions of the Jensen model

2.3.2 Multizone Model

The multizone wake model [6] can be considered a direct extension of the Jensen model. While it retains the core assumption of a wake radius that expands linearly with downstream distance, it introduces a more refined representation of the wake structure by dividing it into three distinct zones. Each of these zones is characterized by a different wake expansion coefficient, allowing for a more accurate modelling of the wake's spatial evolution.

The regions are:

- near wake,
- far wake
- mixing zone

Here is a schematic representation of the model:

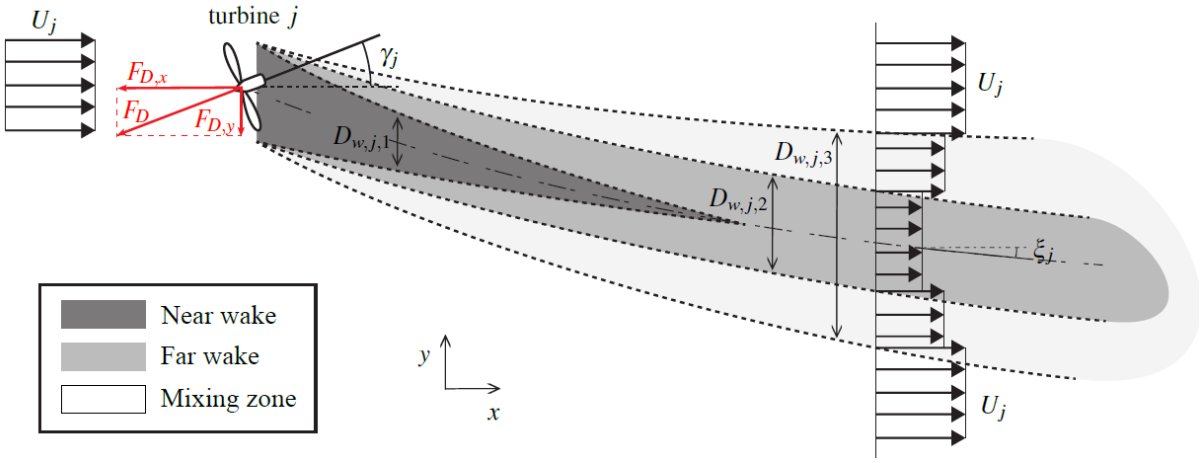

Figure 5 - top view of the model representation

In the image above $D_{w,j,1}$, $D_{w,j,2}$ and $D_{w,j,3}$ refer to the diameters of each expanding zone. These diameters are determined using the following relations:

$$D_{w,j,q}(x) = max\left(D_j + 2k_e m_{e,q} x, 0\right) \tag{4}$$

where the index q takes on the values 1, 2, and 3 for the near wake, far wake, and mixing zone, respectively, D_j is the diameter of turbine j, the parameters $m_{e,q}$ and k_e characterize the wake's expansion. Once the size of each region is established, the velocity deficit is computed

assuming a quadratic decay with respect to the downstream distance from the rotor. The velocity distribution in the wake generated by turbine j can be expressed as:

$$U_{w,j}(x,r) = U_j\left[1 - 2a_j c_j(x,r)\right] \tag{5}$$

where a_j represents the axial induction factor, while x and r denote the axial and radial distances from the centre of the wake. Additionally, the coefficient c_j is the wake decay coefficient which has different values depending on the region:

$$c_j(x,r) = \begin{cases} c_{j,1} & \text{if} \quad r \le D_{w,j,1}/2 \\ c_{j,2} & \text{if} \quad D_{w,j,1}/2 < r \le D_{w,j,2}/2 \\ c_{j,3} & \text{if} \quad D_{w,j,2}/2 < r \le D_{w,j,3}/2 \\ 0 & \text{if} \quad r > D_{w,j,3}/2 \end{cases} \tag{6}$$

The local wake decay coefficient for each region can be calculated with:

$$c_{j,q}(x) = \left[\frac{D_j}{D_j + 2k_e m_{U,q}(\gamma_j)x}\right]^2 \tag{7}$$

The parameter $m_{U,q}$ is a function of γ_j to account for rotor yaw angle. It is possible to express it with this relationship derived empirically:

$$m_{U,q}(\gamma_j) = \frac{M_{U,q}}{\cos(a_U + b_U\gamma_j)} \tag{8}$$

with parameters $M_{U,q}, a_U, b_U$ calibrated by fitting the model to the downstream turbine power output obtained from high-fidelity simulations using SOWFA (Simulator fOr Wind Farm Applications), a CFD simulator of wind flow around turbines in the ABL (Atmospheric Boundary Layer).

2.3.3 Bastankhah and Porté-Agel deficit Model

The model will be discussed in greater detail later, in the section dedicated to wake deflection. For now, it is important to note that the authors began their analysis from the integral forms of the Reynolds-Averaged Navier–Stokes (RANS) equations. Using high-resolution velocity field measurements in the wake of a wind turbine, they systematically evaluated each term in the RANS equations, determining the relative contribution of each to the overall momentum balance. This detailed assessment revealed that certain terms could be neglected, as their influence on the studied phenomenon was minimal. As a result, the governing equations were reduced to a simplified set of integral equations, retaining only the dominant physical mechanisms.

Furthermore, by assuming that the streamwise velocity deficit can be idealized as a Gaussian distribution, the authors were able to derive an analytical expression for the velocity deficit in the streamwise direction, given by:

$$\frac{\Delta\bar{u}}{\bar{u}_\infty} = \left(1 - \sqrt{1 - \frac{C_T \cos\,\gamma}{8\left(\sigma_y \sigma_z / d^2\right)}}\right) \mathrm{e}^{-0.5\left((y-\delta)/\sigma_y\right)^2} \mathrm{e}^{-0.5\left((z-z_h)/\sigma_z\right)^2} \tag{9}$$

where C_T is the coefficient of thrust, σ_y and σ_z represent the wake width respectively in the y and z direction, $\bar{u}_\infty$ indicates the mean speed of the incoming wind and γ represents the yaw angle.

The following images, Figure 6 and Figure 7, clearly illustrate the development of the downstream velocity deficit. A clear increase in wake deflection is observed in Figure 6 with increasing yaw misalignment. This effect is evident from the progressive lateral displacement of the wake centreline, which is identified by the red markers.

In Figure 7, it can also be seen that the assumption of self-similar velocity profiles holds true, at least in the case of the far wake, where the flow exhibits a consistent shape when normalized appropriately.

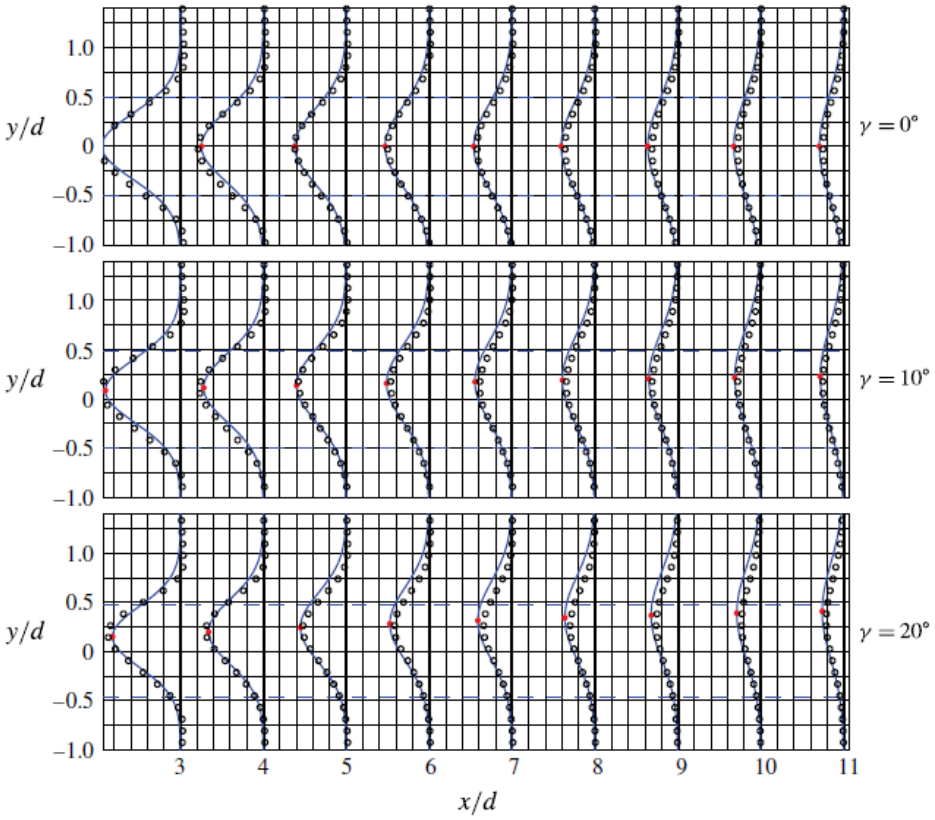

Figure 6 - lateral profiles of the normalized mean streamwise velocity $\bar{u}/\bar{u}_h$ ($\bar{u}_h$ is the incoming velocity at the hub height of the turbine) at different yaw angles [4]. Wind tunnel measurements (open black circle) are plotted against the model predictions (blue lines). Horizontal dashed lines indicate the projections of the side tips of the turbine. Red dots indicate the position of the wake centre position predicted by the model. Each vertical thick black line corresponds to a value of 1 for the normalized streamwise velocity. The width of grid squares corresponds to 15% of $\bar{u}_h$

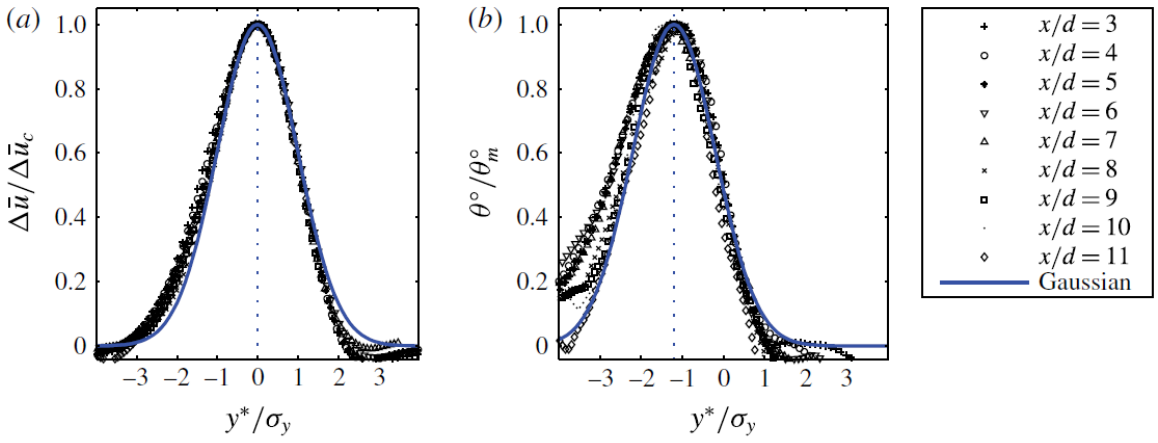

Figure 7- self similar lateral profiles at different downwind position of a wake originated from a turbine with $\gamma = 30°$. The model is compared against experimental data. (a) velocity deficit $\Delta\bar{u}$ profiles normalized by the maximum velocity deficit $\Delta\bar{u}_c$ against y^*/σ_y, where σ_y is the width of the wake in the y direction and y^* is the lateral distance from the wake centre. (b) wake skew angle θ normalized by the maximum skew angle at each downwind location θ_m against y^*/σ_y

2.4 Wake deflection models

In the previous section the models that address the distribution of the velocity deficit were presented. Nevertheless, velocity deficit formulations are just one of the main components of a wake model as a whole. It has been said that a wake has also lateral displacement that should be accounted for. That said, in this section the formulations that model such deflection are going to be presented. It is important to emphasize that this analysis does not aim to provide a comprehensive or exhaustive overview of all existing models. Only a selection will be presented here. Before giving a detailed description of each one of them, here is a summary:

- Jiménez model, obtains the deflection through momentum conservation equations
- Bastankhah and Porté-Agel model, obtains the deflection through the integral form of RANS equations and by assuming a Gaussian velocity deficit profile

In the following paragraphs the models will be presented in more detail.

2.4.1 Jiménez deflection model

To fully characterize the flow field, including the turbulent structures in the wake region, a Direct Numerical Simulation (DNS) would be required. However, such an approach becomes practically unfeasible for industrial applications due to the extremely high computational cost associated with simulating flows at high Reynolds numbers.

For this reason, hybrid turbulence modelling approaches such as Large Eddy Simulation (LES) have been developed. In LES, only the smaller scales of turbulence, those most affected by viscous dissipation, are modelled, while the larger, energy-containing eddies are directly resolved by the numerical scheme.

This is precisely the approach adopted by Jimenez et al. [7]. In their study, a LES model with periodic boundary conditions was implemented within a computational fluid dynamics (CFD) code to simulate the turbulence generated in the wake region.

The turbine model employed in this study recalls a porous disk approach. Specifically, the rotor is represented as a set of rectangular cells embedded within a Cartesian computational grid. Each of these cells is associated with a localized momentum sink such that the total momentum extracted from the flow matches the prediction given by the classical actuator disk theory.

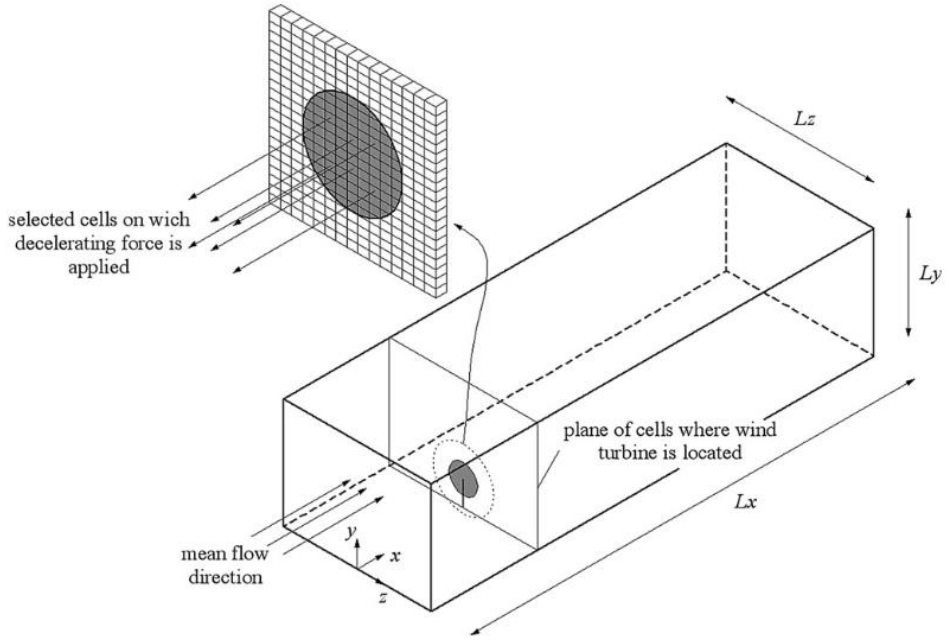

Figure 8 - computational domain used in [7]

The primary reason for using such a simplified model, which does not resolve the detailed blade-flow interactions, is that the focus of the study lies not in the near-wake region, but in the far wake. The objective is to characterize the contribution of turbulence within the annular shear layer that surrounds the wake, rather than resolving the fine-scale flow features in the immediate vicinity of the blades. In the absence of yaw misalignment, the force applied within the disk cells, opposing the incoming flow, can be expressed as:

$$f_x = -C_T \cdot \frac{1}{2}\rho A U_0^2 \tag{10}$$

where:

- f_x is the force applied to the flow,
- A is the frontal area of the rotor disk,
- C_T is the thrust coefficient,
- U_0 is the average freestream velocity at disk centre position,

When yaw misalignment is present, the force vector is rotated and can be expressed as:

$$f = C_T \cdot \frac{1}{2}\rho A (U_0 \cos\,\theta)^2 \tag{11}$$

where:

- θ represents the yaw angle

The components of this force in the reference frame used for the simulation are then given by:

$$f_x = -f\cos\,\theta = -C_T \cdot \frac{1}{2}\rho A(U_0\cos\,\theta)^2\cos\,\theta$$
$$f_z = -f\sin\,\theta = -C_T \cdot \frac{1}{2}\rho A(U_0\cos\,\theta)^2\sin\,\theta \quad (12)$$

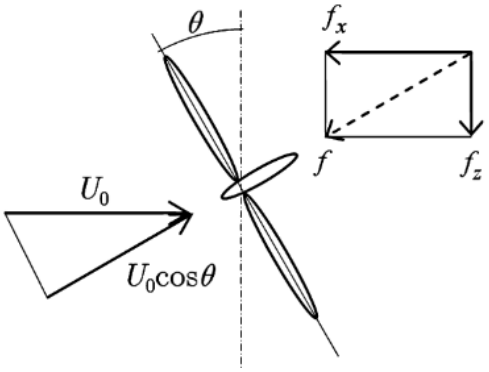

Figure 9 - aerodynamic force in the presence of yaw misalignment

Now, starting from the formulations obtained, the next step is to obtain an expression for the force exerted at generic downwind distance. To do that a few simplifications are made:

- The model to calculate the wake deflection δ is based on a top hat model. That means that inside a cross-section of the wake the velocity is considered uniform and inclined with angle α, the skew angle.
- The control volume will be taken sufficiently far from the turbine so that the pressure field is in first approximation uniform
- the error of considering $U_0 - \Delta U = U_0$ is negligible, where ΔU is the velocity deficit in the wake
- α, the skew angle, should be small enough to approximate $\cos\,\alpha = 1$ and $\sin\,\alpha = \alpha$

With these hypotheses, by applying the momentum conservation, the following relationships are obtained:

$$f_x \approx -\rho U_0 \Delta U \frac{\pi\delta^2}{4}$$
$$f_z \approx -\rho U_0^2 \frac{\pi\delta^2}{4}\alpha \quad (13)$$

The value of α can be obtained as a function of δ:

$$\alpha = \left(\frac{D}{\delta}\right)^2 \cos^2\,\theta\sin\,\theta\frac{C_T}{2} \quad (14)$$

By assuming $\delta = D$, the initial skew angle of the wake can be expressed as:

$$\alpha|_{x-0} = \cos^2\ \theta \sin\ \theta \frac{C_T}{2} \tag{15}$$

If we suppose a linear increase in the wake cross-section with downstream distance x, so that $\delta = D + \beta x$, where β is a coefficient related to the wake growth, then the skew angle expression can be further developed into:

$$\alpha = \frac{\cos^2\ \theta \sin\ \theta \frac{C_T}{2}}{\left(1 + \beta \frac{x}{D}\right)^2} \tag{16}$$

If we, as explained by Gebraad et al. [6], integrate the tangent of the wake centreline angle over x, the yaw-induced lateral offset of the wake center with respect to the hub of turbine j can be expressed as:

$$y_{w,yaw,j}(x) \approx \int_0^x \tan\left(\alpha_j(x)\right) dx \tag{17}$$

This integral can be approximated by integrating the second order Taylor series approximation of $\alpha(x)$, yielding:

$$y_{w,yaw,j}(x) \approx \frac{\tilde{C}_T(a_j, \gamma_j)\left[15\left[\frac{2xk_d}{D} + 1\right]^4 + \tilde{C}_T(a_j, \gamma_j)^2\right]}{\frac{30k_d}{D}\left[\frac{2xk_d}{D} + 1\right]^5}\Bigg|_0^x \tag{18}$$

with $\tilde{C}_T(a_j, \gamma_j)$ is equal to $\frac{1}{2}\cos^2\left(\gamma_j\right)\sin\left(\gamma_j\right)C_T(a_j)$ and k_d is a model parameter that defines the sensitivity of the wake deflection to yaw. The following is an image that represents the wake shape and the meaning of the variables presented in this section:

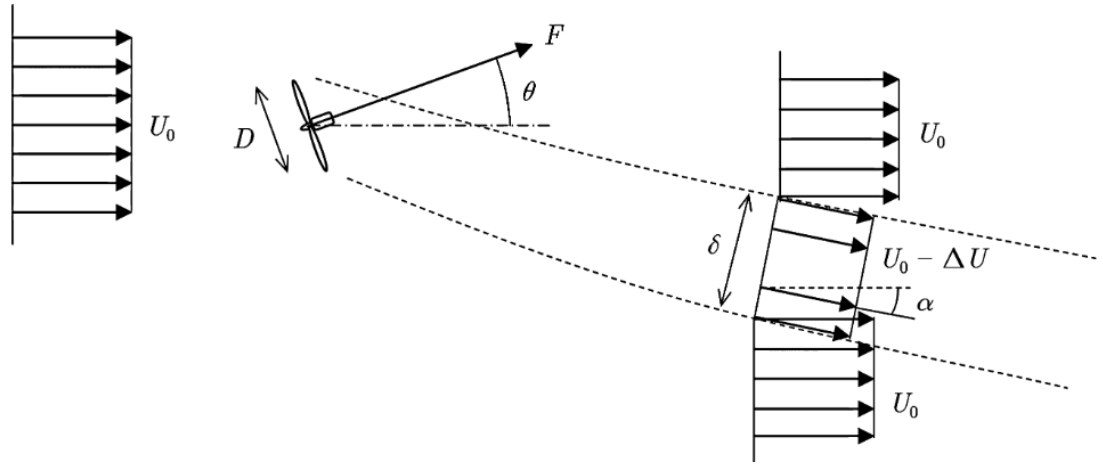

Figure 10 - schematic representation of the Jimenéz model

2.4.2 Bastankhah and Porté-Agel deflection model

Bastankhah and Porté-Agel conducted a detailed investigation of the wakes generated by yawed wind turbines using wind tunnel experiments under neutrally stratified boundary layer conditions [8]. High-resolution spatial velocity measurements enabled a systematic analysis of the wake structure and evolution. The following image illustrates the experiments conducted:

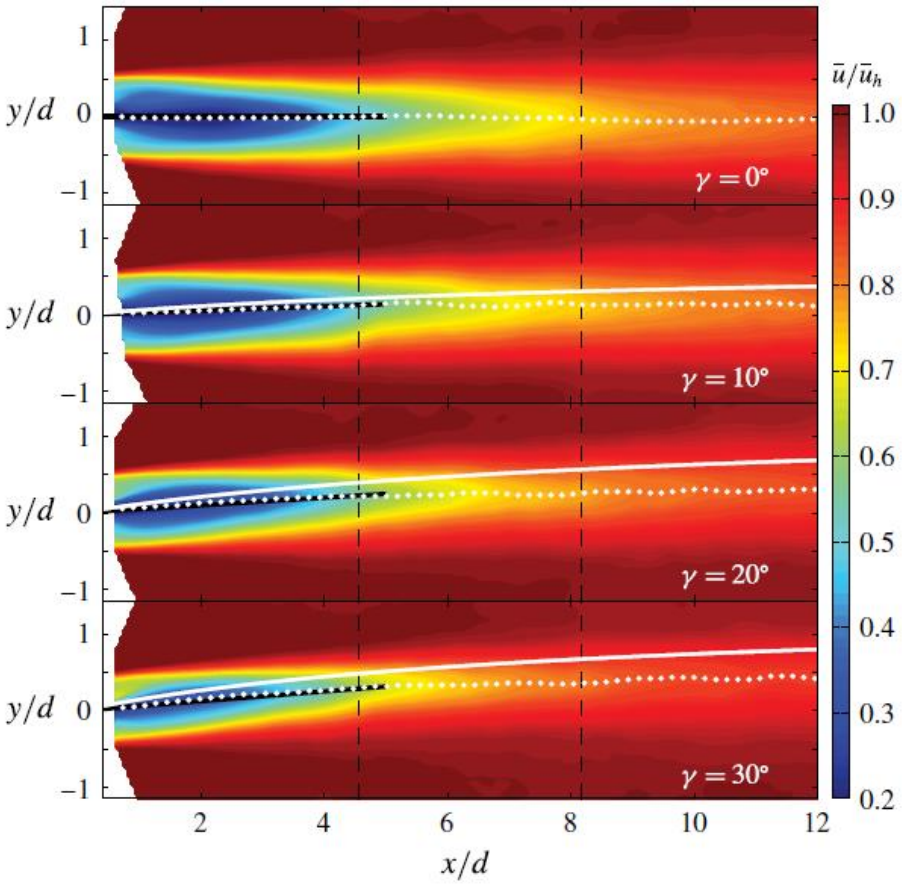

Figure 11 - contours of the normalized mean streamwise velocity in the horizontal plane at hub height at optimal tip-speed ratio λ_o [8]

The experimental data obtained were then used to perform budget analysis of the Reynolds-Averaged Navier–Stokes (RANS) equations. This approach allowed the researchers to identify and isolate the dominant terms contributing to the wake dynamics. Based on these insights, they were able to derive simplified governing equations. The first assumption introduced to simplify the analytical formulation is that both the velocity deficit and the skew angle profiles in the lateral (y) direction can be represented using Gaussian distributions. The validity of such assumption can be seen in Figure 7.

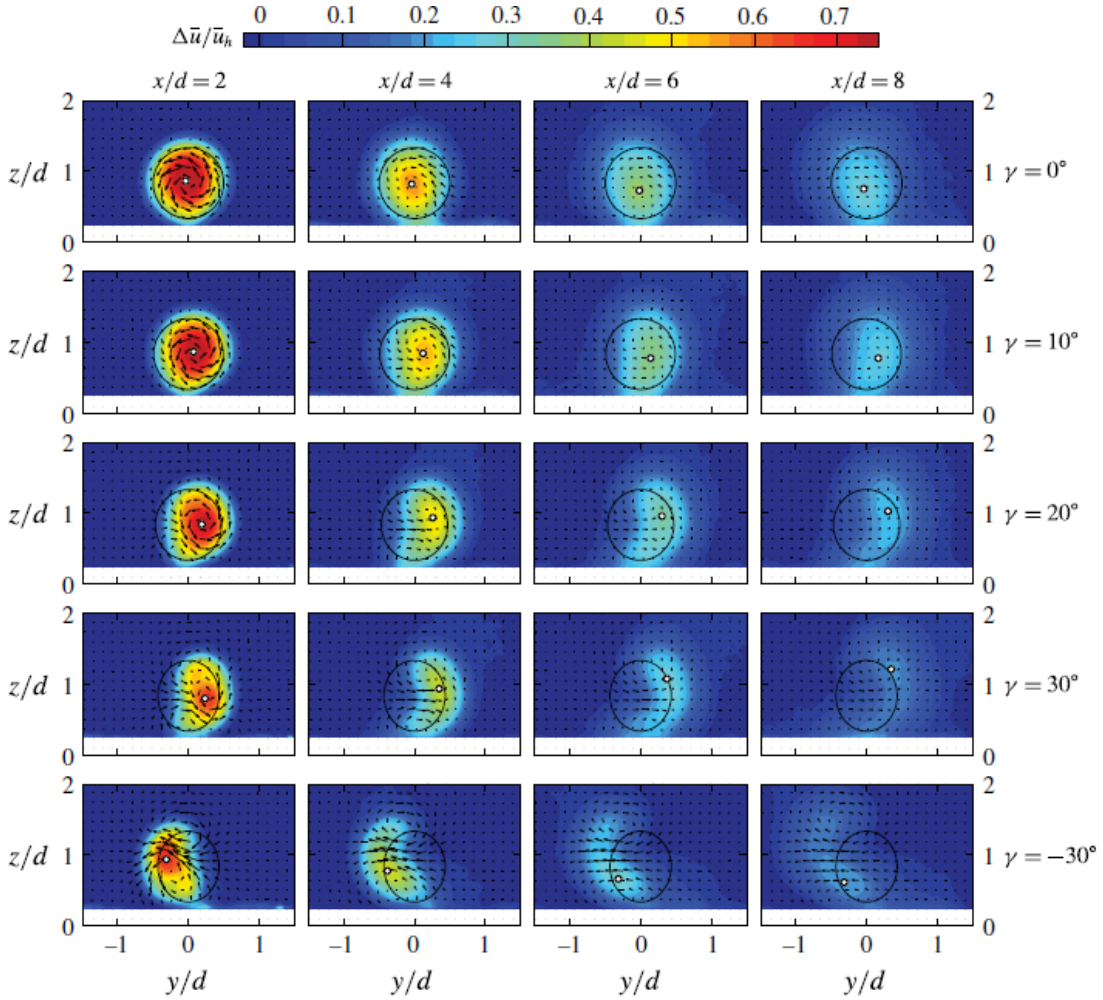

Figure 12 – normalized streamwise velocity deficit with different yaw angles and different downwind locations for a turbine operating at optimal tip-speed ratio λ_o [8]

Although the velocity deficit in the vertical (z) direction generally requires a more detailed treatment, primarily due to the presence of counter-rotating vortex pairs (CVPs), which distort the vertical velocity distribution into a characteristic kidney-shaped pattern, these effects become negligible for small yaw misalignment angles. Under such conditions, it is reasonable to also approximate the vertical distribution using a Gaussian profile. As a result, both the velocity and skew angle distributions can be formulated as follows:

$$\left.\begin{aligned}\frac{\bar{u}(x,y,z)}{\bar{u}_\infty} &= 1 - C\mathrm{e}^{-(y-\delta)^2/2\sigma_y^2}\mathrm{e}^{-(z-z_h)^2/2\sigma_z^2},\\ \frac{\theta(x,y,z)}{\theta_m} &= \mathrm{e}^{-(y-\delta+\sigma_y)^2/2\sigma_y^2}\mathrm{e}^{-(z-z_h)^2/2\sigma_z^2},\end{aligned}\right\} \tag{19}$$

where C is the normalized velocity deficit at wake centre, δ is the wake centre deflection and σ_y and σ_z represent the wake width respectively in the y and z direction.

Inserting the equation found in the integral form of the RANS equation along the spanwise direction and integrating, yields:

$$\frac{2\pi\bar{u}_\infty^2}{3e^{1/3}}\frac{d}{dx}\left[\theta_m\sigma_y\sigma_z\left(C^2-3e^{1/12}C+3e^{1/3}\right)\right]=0 \tag{20}$$

and the wake skew angle of the wake centre $\theta_c(\theta_c=\theta_m e^{-0.5})$ can be written as

$$\theta_c=\frac{\theta_{c_0}\left(\sigma_{y_0}\sigma_{z_0}\right)E_0}{\sigma_y\sigma_z(C^2-3e^{1/12}C+3e^{1/3})} \tag{21}$$

where $E_0=C_0^2-3e^{1/12}C_0+3e^{1/3}$. The "0" subscript refers to quantities at the far wake onset. After integrating and some algebraic manipulation, the wake deflection can be written as a function of the wake characteristics at the onset of the far-wake and the rates of wake expansion k_y and k_z.

$$\delta=\delta_0+\frac{\theta_{c_0}E_0}{5.2}\sqrt{\frac{\sigma_{y_0}\sigma_{z_0}}{k_yk_zM_0}}\ln\left[\frac{\left(1.6+\sqrt{M_0}\right)\left(1.6\sqrt{\frac{\sigma_y\sigma_z}{\sigma_{y_0}\sigma_{z_0}}}-\sqrt{M_0}\right)}{\left(1.6-\sqrt{M_0}\right)\left(1.6\sqrt{\frac{\sigma_y\sigma_z}{\sigma_{y_0}\sigma_{z_0}}}+\sqrt{M_0}\right)}\right] \tag{22}$$

In this equation M_0 is equal to $C_0(2-C_0)$. The equation considers the characteristics at the onset of the far-wake. To have a better understanding of what this means, it is useful to represent the evolution of the wake with the assumptions of the present model:

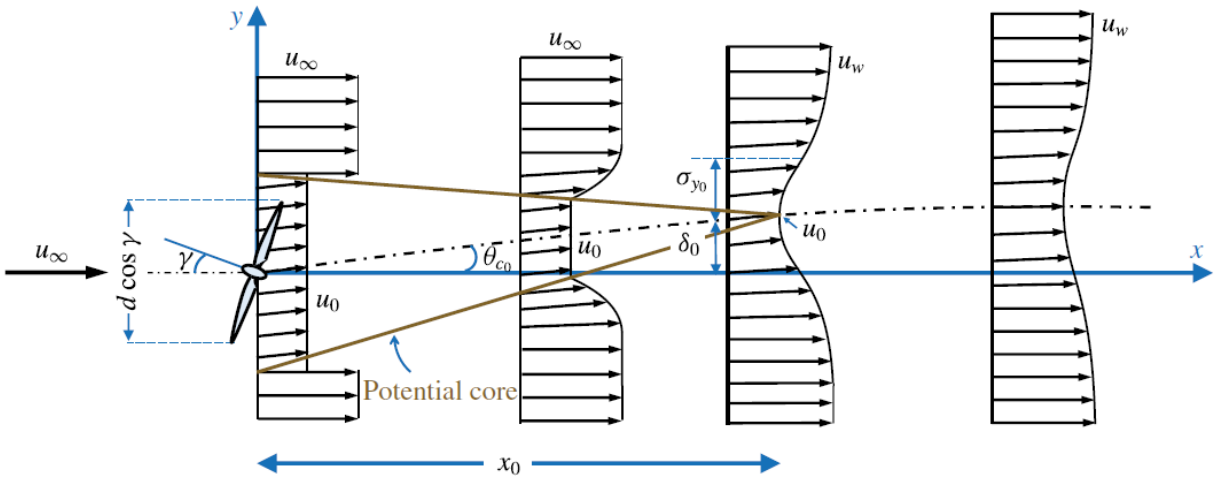

Figure 13 - schematic representation of the wake where the boundaries of the potential core can be seen [8]

Bastankhah and Porté-Agel adopted the concept of a potential core from co-flowing jet theory to describe the near-wake region behind a wind turbine. The potential core is defined as a region immediately downstream of the rotor where the flow remains uniform in velocity.

This uniform core gradually decreases in size with increasing downstream distance. At a certain point, the potential core fully dissipates, and the wake transitions into a region where the velocity field becomes self-similar and can be accurately described using a Gaussian distribution. Therefore, the onset variables of the far wake are defined at the boundary between the potential core and the self-similar Gaussian flow region. The idealization of the potential core was not intended to provide a detailed representation of the near wake, which is highly complex and characterized by strong turbulence, rotational effects, and non-uniform velocity fields. Instead, the purpose of introducing the potential core concept is to establish a well-defined and physically consistent transition point from which the far-wake model can be initialized. This enables the analytical formulation of the wake deflection and velocity deficit profiles starting from known initial conditions at the end of the potential core region. By defining the onset conditions at this location, the far-wake behaviour can be predicted.

In the study of Bastankhah and Porté-Agel the far wake onset variables are calculated as follows:

$$\begin{cases} \dfrac{u_0}{u_\infty} = \sqrt{1 - C_T} \\ \dfrac{\sigma_{y_0}}{d} = \dfrac{\sigma_{z_0}}{d} \cos\gamma \\ \delta_0 = x_0 \tan\vartheta_{c_0} \cong x_0 \vartheta_{c_0} \\ \dfrac{x_0}{d} = \dfrac{\cos\ \gamma\left(1 + \sqrt{1 - C_T}\right)}{\sqrt{2}\left[4\alpha I + 2\beta\left(1 - \sqrt{1 - C_T}\right)\right]} \end{cases} \tag{23}$$

Where x_0 is the length of the potential core, as can be seen in Figure 13. α and β are constants that should be estimated. Bastankhah and Porté-Agel [8] determine β based on analogy with jet flows. If 2β is equal to 0.154, the $\frac{x_0}{d}$ equation of (23) gives a similar value of x_0 as the one reported in studies of jet flows in the case of ideal conditions with no incoming turbulence. The value of α can be consequently obtained by fitting equation $\frac{x_0}{d}$ of (23) to experimental measurements. The authors specify that more numerical simulations or wind tunnel measurements should be carried out to estimate universal values for α and β.

2.5 Turbulence models

In the previous sections the wake model components that account for deflection and velocity deficit were presented. Referring to the definition of wake, as the altered region downstream a turbine with reduced velocity and increased turbulence, it becomes clear that one of the main aspects to consider in wake modelling is turbulence, other than spatial evolution. This paragraph is dedicated to analysing this phenomenon in the context of wind turbines.

Turbulence refers to fluid motion characterized by chaotic changes in pressure and flow velocity. The airflow approaching a wind turbine is inherently turbulent, with fluctuations in wind speed driven by the production of turbulent kinetic energy. This energy arises due to surface roughness of the ground and is further influenced by atmospheric stability, enhancing or dampening turbulence levels. When wind passes through the rotor of a wind turbine, its turbulence intensity increases due to several physical mechanisms. Two primary contributors to this turbulence enhancement are:

- Rotor-induced swirl: The rotation of the turbine blades imparts angular momentum to the flow, introducing rotational disturbances and contributing to increased turbulence levels in the wake.
- Kinetic energy extraction: As the turbine extracts energy from the wind, a velocity deficit forms behind the rotor. This creates shear layers between the slower wake flow and the faster surrounding free stream, which are inherently unstable and lead to turbulence generation.

Since turbulence is an extremely complex and multi-scale phenomenon, several models have been developed to lessen the computational cost of simulations. A common model used to describe added turbulence is the Crespo-Hernández Model [9]. This method takes into consideration both the background atmospheric turbulence and the extra turbulence introduced by the spinning blades of the turbine. It describes the added turbulence as dependent on several factors: the axial induction factor, the turbulence intensity of the incoming wind, and the distance downstream from the turbine. The model is based on results from wind tunnel testing and aligns well with computational fluid dynamics (CFD) simulations.

2.6 Wake combination models

In a wind farm, where many wind turbines operate, multiple wakes interact with each other overlapping and influencing downstream turbines. When this occurs, the actual reduction in wind speed results from the combined effect of the overlapping wakes.

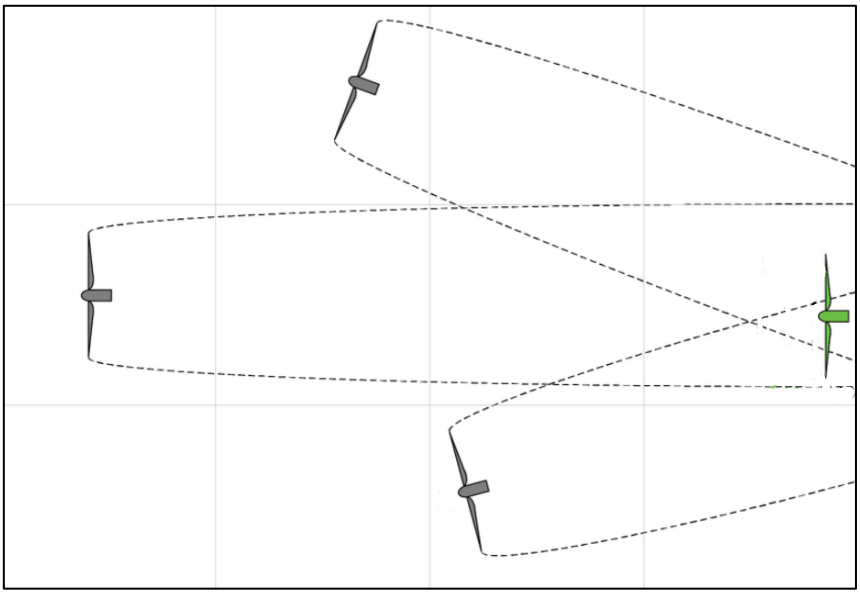

Figure 14 - schematic representation of wake overlapping [10]

There are several methods for estimating the combined impact of multiple wakes:

- Linear superposition: it involves summing all individual velocity deficits equally. This method assumes each wake has the same weight in the final result, regardless of its origin.
- Quadratic summation (sum of squares method): This technique calculates the overall velocity deficit by taking the square root of the sum of the squares of the individual wake deficits. Compared to the previous method, this one tends to provide a more accurate estimation of the combined wake effects, particularly in low-fidelity wind farm models.

2.7 Parametric dynamic wake models

The models presented so far have been extensively used in steady-state tools, among which FLORIS [11] and PyWave [12] are notable examples. These models have gained widespread adoption due to their very low computational cost and relatively high accuracy in static conditions. However, they share a fundamental shortcoming: they do not account for dynamic effects. This means that changes in operational conditions of the turbine or in wind conditions instantaneously alter the entire wake, in accordance with the steady-state assumption. However, the dynamic propagation and evolution of the wake can give useful insights that can contribute to more complete and realistic wind farm layout design tools, control strategies and large-scale wind farm simulations. Therefore, to overcome the steady-state limitation, several dynamic modelling approaches have been developed over time, aiming to incorporate more realistic representations of transient behaviours in wind farm flow interactions.

As highlighted by M. Becker et al. [13], multiple research tracks can be identified in the study of dynamic wake modelling.

Here is a brief timeline of the first major research trail:

- 2010: The development begins with the Aeolus SimWindFarm toolbox [14]. This model had several limitations: it was two-dimensional, and it assumed fixed mean wind speed, wind direction, and yaw angle. Despite these simplifications, it successfully reproduced the wake meandering [1] effect through the use of passive tracers.
- 2014: Poushpas and Leithead extended the Frandsen wake model [15] by incorporating a dynamic turbine framework. This enhancement aimed to enable more accurate estimation of fatigue loads by introducing turbine dynamics into the simulation.
- 2018: Bossanyi introduced the Dynamic Wind Farm Simulator [16], a modelling framework designed to capture the dynamic interactions within wind farms. The model leverages the in-house Bladed code to establish a link between yaw misalignment and the power coefficient (Cp). Furthermore, the simulator extends its capabilities by incorporating wake steering into the control strategy, allowing for active redirection of wakes to optimize overall farm performance. For modelling wake deflection, the simulator adopts the approach proposed by Jiménez et al. [7], which provides an

[1] The wake meandering effect refers to the lateral and vertical oscillation of the wake over time. This phenomenon is primarily caused by turbulent large-scale structures in the atmospheric boundary layer and unsteady interactions between the wake and the surrounding flow, leading to time-dependent displacement of the wake centreline.

analytical description of the lateral displacement of wakes due to yawed turbine operation.

The second trail of publications follows this timeline:

- 2017: Shapiro et al. [17] employed the Jensen wake deficit model, coupled with an induction control strategy, to represent the dynamic extraction of kinetic energy by wind turbines. Building upon the conservation laws of momentum and mass, the authors derived a linear advection velocity law to describe the downstream propagation of the wake. The model operates under the assumption of constant wind speed and direction, which simplifies the governing dynamics but limits realism under varying atmospheric conditions. This approach does also not account for yaw variations, nor does it include the dependency of the wake expansion factor (i.e. a parameter estimating the relationship between downstream distance and the increasing wake radius) on the thrust coefficient (Ct).
- 2018: Shapiro et al. [18] later extended their previously introduced model to also account for variations in yaw angle.
- 2021: Kheirabadi and Nagamune [19] introduced the Floating Offshore Wind Farm Simulator, taking inspiration from the cited previous work and extending it to offshore wind turbine systems. The authors incorporated the dynamics of floating platforms including mooring line effects to capture the motion of offshore turbines under environmental loading. In addition, the model accounts for time-varying free-stream wind conditions, enabling a more realistic representation of unsteady inflow and its impact on turbine performance and wake behaviour. The wake modelling is based on the previously discussed Gaussian wake deficit model.

The third trail of publications is here presented:

- 2014: Gebraad and van Wingerden [20] developed FLORIDyn, a dynamic extension of the FLORIS model (FLOw Redirection and Induction in Steady-state, Gebraad et al., 2014) [11] .The core idea behind FLORIDyn is as follows: At each time step, an array of points, referred to as Observation Points (OPs), is generated at the rotor plane of each turbine. These OPs inherit the turbine's state variables, such as yaw angle and induction factor. In subsequent time steps, the OPs travel downstream at their respective effective velocities at hub height, thereby propagating wake dynamics toward downstream

turbines. Despite its contribution to dynamic wake modelling, FLORIDyn has certain limitations: it is two-dimensional, and it does not account for variations in wind direction.

- 2022: M. Becker et al. [13] developed a revised version of the FLORIDyn tool, aiming to overcome the limitations of the original implementation. This updated version can process three-dimensional wind fields and integrates a Gaussian wake model [8], providing a more accurate and flexible representation of wake dynamics. In addition, it introduces the capability to handle heterogeneous and time-varying wind conditions, including the effects of wind shear and added turbulence, which are critical for realistic simulation of atmospheric flow and wake interactions across a wind farm.

It is precisely this version of the FLORIDyn model that will be used for the implementation within the tool MOST. Accordingly, the next chapter will provide a detailed description of the revised FLORIDyn model.

CHAPTER 3. COMPUTATIONAL FRAMEWORK - FLORIDyn

3.1 Introduction on FLORIDyn

FLORIDyn (FLOw Redirection and Induction Dynamics) [13] is the selected model for extending the capabilities of MOST, specifically to enable modelling of wake dynamics.
FLORIDyn is a three-dimensional parametric Gaussian model that builds upon and extends the functionalities of the FLORIS tool [11]. While FLORIS neglects dynamic variations in wind conditions and turbine yaw, FLORIDyn accounts for these effects by introducing a low-computational-cost framework that incorporates such dynamics.
To achieve this, FLORIDyn introduces the concept of Observation Points (OPs), whose detailed definition will be provided later. At each time step, a set of OPs is generated at the rotor plane of each turbine. These OPs inherit the turbine's current state. By doing so, dynamic variations can be propagated downstream over time. The coordinates of the OPs are mathematically mapped to the global (world) reference frame, allowing for the correct spatial tracking and evolution of wake effects.

3.2 Wake model

As previously mentioned, FLORIDyn is developed based on the wake deflection and velocity deficit model proposed by Bastankhah and Porté-Agel [8]. This model is extended through the incorporation of added turbulence calculations, following the approach introduced by Crespo and Hernández [9]. Figure 15 is a schematic representation of the spatial evolution of the wake, clearly illustrating the transition between the near wake, the potential core, and the far wake regions:

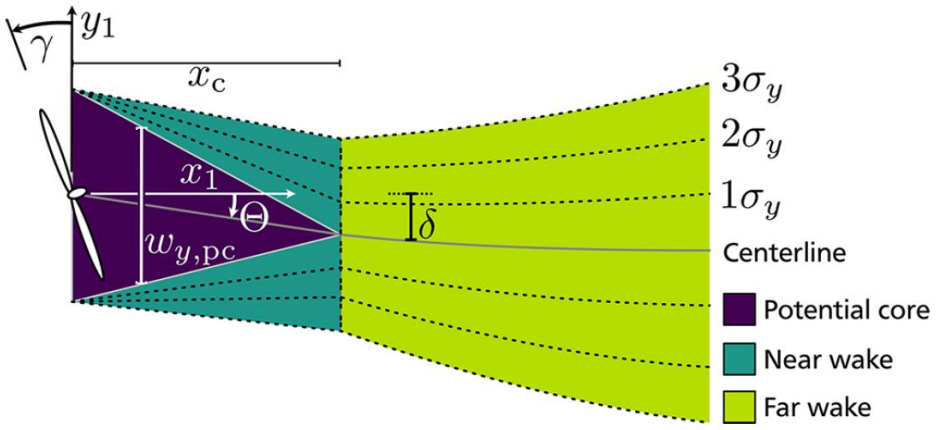

Figure 15 - schematic representation of the Gaussian wake [13]

It is clear in the above figure the distribution of the different zones. The reduction factor of the potential core is constant and sets the boundary with the near wake area. When the potential core fades, that cross section is the starting point of the far wake. The model uses two coordinate systems, one for the wake K_1, which centre lays on the rotor, and one world coordinate system K_0. In the figure the x_1 axis belongs to the wake coordinate system, indicating the direction of downstream propagation. The symbol Θ indicates the wake deflection angle, called skew angle, and δ is the local wake deflection, which gives the position of the centreline of the wake. The potential core widths in the y direction and z direction are indicated with $w_{y,pc}$ and $w_{z,pc}$, whereas the widths of the near wake and far wake area are indicated with σ_y and σ_z. To cover most of the wake influence it was decided to set the actual wake widths to $\pm 3\sigma_y$ and $\pm 3\sigma_z$.
For the three regions of interest, a reduction factor can be computed, defined as:

$$r = \frac{\Delta u}{u_{\text{free}}} \tag{24}$$

3.3 Observation Points

Within the FLORIdyn framework, in order to simulate the downstream propagation of wake modifications induced by dynamic changes in the turbine operating state, the concept of Observation Points (OPs) is introduced.
An Observation Point can be interpreted as a representative mass of air that travels downstream at a certain velocity. It serves as a moving reference that allows the tracking of wake

characteristics as they evolve over time and space, capturing the dynamic response of the wake to unsteady turbine behaviour.

The rotor is modelled as a porous disk. At each simulation time step, a set of Observation Points is generated at the rotor location, following a sunflower distribution [21]. The algorithm returns relative coordinates $(v_y, v_z) \in [-0.5,0.5]$ which will further be used as a distribution, to retrieve OPs coordinates.

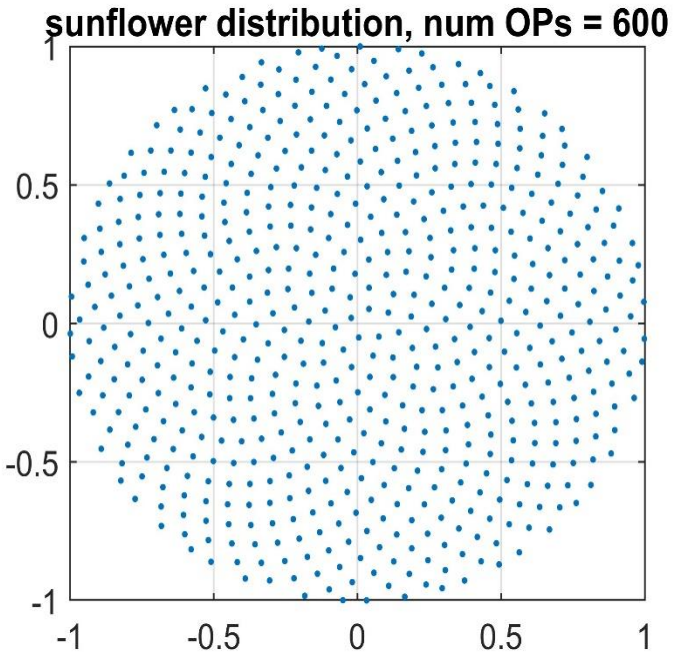

Figure 16 - sunflower distribution of the OPs created at the turbine rotor

In subsequent time steps, these OPs travel downstream at the freestream velocity. The reason behind using a constant convection speed, rather than the actual local flow conditions, will be discussed in a later section.

From an implementation standpoint, each OP is part of a data structure that stores both its position in the global reference frame and the turbine's operational state at the time of the OP's creation. The downstream propagation of the OPs is performed by passing their spatial distribution and associated turbine state data to an algorithm based on a Gaussian wake model. Because each OP retains the turbine state from the moment it was created, the propagation model can determine its trajectory based on localized input. The Gaussian wake algorithm, therefore, evolves each OP's position using the specific conditions under which it originated.

An example is provided below. In panels (a) and (b), the creation and subsequent movement of the OPs are shown. Panels (c) and (d) depict a change in the turbine's yaw angle. It can be clearly observed that downstream OPs continue to follow trajectories based on the turbine state at their time of origin, whereas newly generated OPs follow paths defined by the Gaussian model applied to the updated turbine parameters.

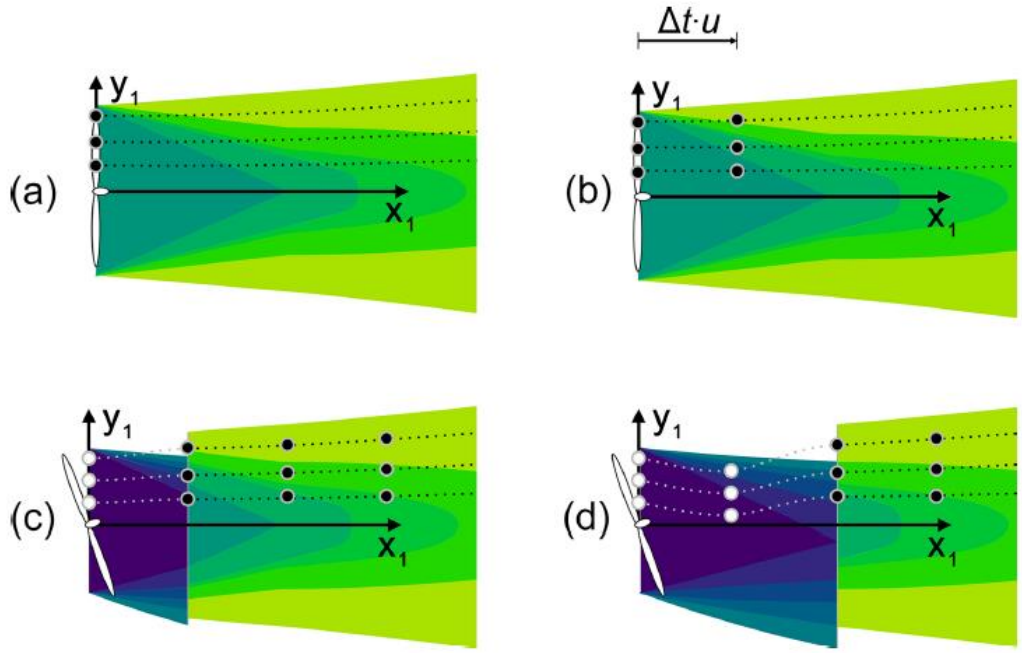

Figure 17 - OPs traveling downwind in the case of turbine yaw change [13]

Another important feature of the framework can be inferred from the image. OPs that originate from the same relative coordinate within the sunflower pattern form what is referred to as a chain. In the image, each chain, comprising all OPs generated from the same relative position on the rotor, is highlighted by a dashed line, which linearly approximates the trajectory of the OPs over time.

It is important to note, however, that this representation is purely visual. The dashed lines serve only as an illustrative aid. OPs are advected in discrete time steps, and there is no continuous tracking or explicit linkage of OPs along a chain within the simulation code.

The position of an OP in the wake coordinate system is computed using the following equations:

$$y_{1,\mathrm{OP}}\left(v_{y,\mathrm{OP}}, \sigma_y, w_{y,\mathrm{pc}}, \delta\right) = v_{y,\mathrm{OP}}\left(6\sigma_y + w_{y,\mathrm{pc}}\right) + \delta, \tag{25}$$

$$z_{1,\mathrm{OP}}\left(v_{z,\mathrm{OP}}, \sigma_z, w_{z,\mathrm{pc}}\right) = v_{z,\mathrm{OP}}\left(6\sigma_z + w_{z,\mathrm{pc}}\right). \tag{26}$$

where:

$$\sigma_y = \begin{cases} \sigma_{y,nw} & per \quad 0 < x_1 \leq x_c \\ \sigma_{y,fw} & per \quad x_1 > x_c \end{cases} \tag{27}$$

$$\sigma_z = \begin{cases} \sigma_{z,nw} & per \quad 0 < x_1 \leq x_c \\ \sigma_{z,fw} & per \quad x_1 > x_c \end{cases} \tag{28}$$

Where x_c is the length of the potential core region on the x_1 axis.

It should be noted that the current model only accounts for deflections in the horizontal x-y plane. As a result, it is not capable of capturing vertical wake deflections, such as those induced by a nonzero tilt angle. To incorporate such effects, Equation (25) (26) would need to be appropriately modified to account for vertical displacement components.

Additionally, all OPs that reach the plane z = 0 are excluded from further consideration in the simulation. This filtering ensures that only physically meaningful OPs, those still within the wake region, are retained for downstream analysis.

3.4 Wind direction change and coordinate systems

It is assumed that the dynamic behaviour of the incoming wind only affects the orientation of the wake, without altering the characteristics of the Gaussian wake model itself, and therefore not impacting the internal structure of the wake. For this reason, two distinct reference frames are adopted, as previously mentioned in earlier sections. These are:

The wake reference frame, denoted as *k1*, in which the properties of the wake are described.

The global reference frame, in which the properties of the free stream flow are defined.

The following image provides a schematic representation of this concept:

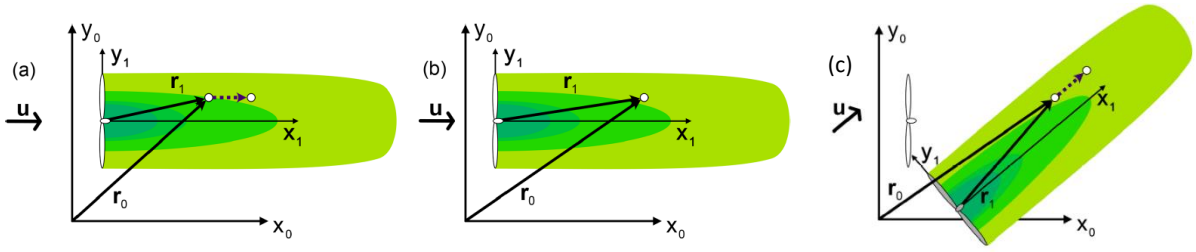

Figure 18 - Observation Point traveling downstream and representation of the position vectors in both the wake (K1) and the global (K0) reference systems. In (a) and (b) the OP travels under a certain wind vector. In (c) the wind direction changes

In Figure 18 the update of the position vector of the Observation Point (OP) under consideration is illustrated. Panels (a) and (b) show the situation where the wind velocity direction remains constant. In contrast, panel (c) shows how a change in wind direction leads to a rotation of the wake reference frame to align with the new wind direction. This rotation results in an apparent displacement of the wake's origin point, even though the turbine's yaw angle has not changed. The coordinates of each OP can be transformed from one reference frame to the other through a rotation-translation. The rotation is defined using the following rotation matrix:

$$\mathbf{R}_{01}(\varphi) = \begin{bmatrix} \cos\,\varphi & -\sin\,\varphi & 0 \\ \sin\,\varphi & \cos\,\varphi & 0 \\ 0 & 0 & 1 \end{bmatrix} \tag{29}$$

Here, φ represents the angle of the OP wind direction, which is, for now, assumed to be uniform across all points. Later it will be shown that each OP can be associated with its own propagation direction.

Therefore, the position vector of an OP in the global reference frame can be expressed as a function of the rotor centre location of the turbine and the position vector of the OP in the wake reference frame:

$$\boldsymbol{r}_0 = \begin{bmatrix} x_0 \\ y_0 \\ z_0 \end{bmatrix} = t_0 + \mathbf{R}_{01}(\varphi)\boldsymbol{r}_1 = \begin{bmatrix} x_{0,\mathrm{T}} \\ y_{0,\mathrm{T}} \\ z_{0,\mathrm{T}} \end{bmatrix} + \begin{bmatrix} \cos\,\varphi & -\sin\,\varphi & 0 \\ \sin\,\varphi & \cos\,\varphi & 0 \\ 0 & 0 & 1 \end{bmatrix} \begin{bmatrix} x_1 \\ y_1 \\ z_1 \end{bmatrix} \tag{30}$$

The advancement step of an Observation Point (OP) is first computed within the wake reference frame k1 using the following expression:

$$x_{1,\mathrm{OP}}(k+1) = x_{1,\mathrm{OP}}(k) + u_{\mathrm{OP}}\Delta t \tag{31}$$

In this equation, k denotes the current time step, and u_{OP} refers to the magnitude of the wind velocity vector $u_{0,\mathrm{OP}}$ at the position $r_{0,\mathrm{OP}}$. The crosswind coordinates can be calculated using expressions (25) (26). This advancement, initially computed in the wake reference frame, can then be transformed into the global reference frame K_0 using the following expression:

$$\boldsymbol{r}_{0,\mathrm{OP}}(k+1) = \boldsymbol{r}_{0,\mathrm{OP}}(k) + \mathbf{R}_{01}\big(\varphi_{0,\mathrm{OP}}\big)\big[\boldsymbol{r}_{1,\mathrm{OP}}(k+1) - \boldsymbol{r}_{1,\mathrm{OP}}(k)\big] \tag{32}$$

Here, $\varphi_{0,\mathrm{OP}}$ represents the local wind direction at the position $\boldsymbol{r}_{0,\mathrm{OP}}(k)$. It is important to note that each OP can have its own local wind direction vector. This capability enables the simulation of non-uniform wind conditions in terms of direction.

3.5 Observation Points travel speed

In terms of propagation velocity, the OPs are assumed to travel downstream with the velocity of the free stream wind. The use of the local effective velocity as the propagation speed was intentionally avoided due to the following issues:

- When comparing the simulation results with high-fidelity SOWFA simulations, assuming the propagation speed to be equal to the local effective velocity leads to a delay in the arrival of state changes at downwind turbines.
- The representation of the wake may no longer remain injective. In other words, the non-uniform propagation of state changes can result in overlapping regions in the same wake

To address these problems, the free-stream velocity was adopted as the propagation speed. This assumption eliminates the issue of self-overlapping wakes by ensuring a consistent and uniform propagation of state changes. However, this approach introduces a new limitation: the state changes propagate more abruptly than what is observed in SOWFA simulations.

This discrepancy is a known issue and highlights a gap between FLORIDyn and high-fidelity models. Bridging this gap will be crucial for improving the accuracy of FLORIDyn in future developments. By addressing these gaps and, potentially, enabling easier tuning of model parameters, FLORIDyn is suitable not only for wind farm layout design under steady-state conditions but also for closed-loop control design applications. This versatility is precisely the reason why FLORIDyn was selected as the core modelling tool for integration within the MOST framework. The implementation details and integration strategy will be discussed extensively in the following chapter.

CHAPTER 4. MODEL IMPLEMENTATION

4.1 Introduction on the MOST implementation of dynamic Gaussian wake model

In the previous chapter, the dynamic modelling approach of FLORIDyn was introduced. The next step, which will be addressed in this chapter, involves the integration of said model into the Simulink environment of MOST. This transition enables the model to be embedded within a larger simulation framework, facilitating modular design and the potential for closed-loop control system integration.

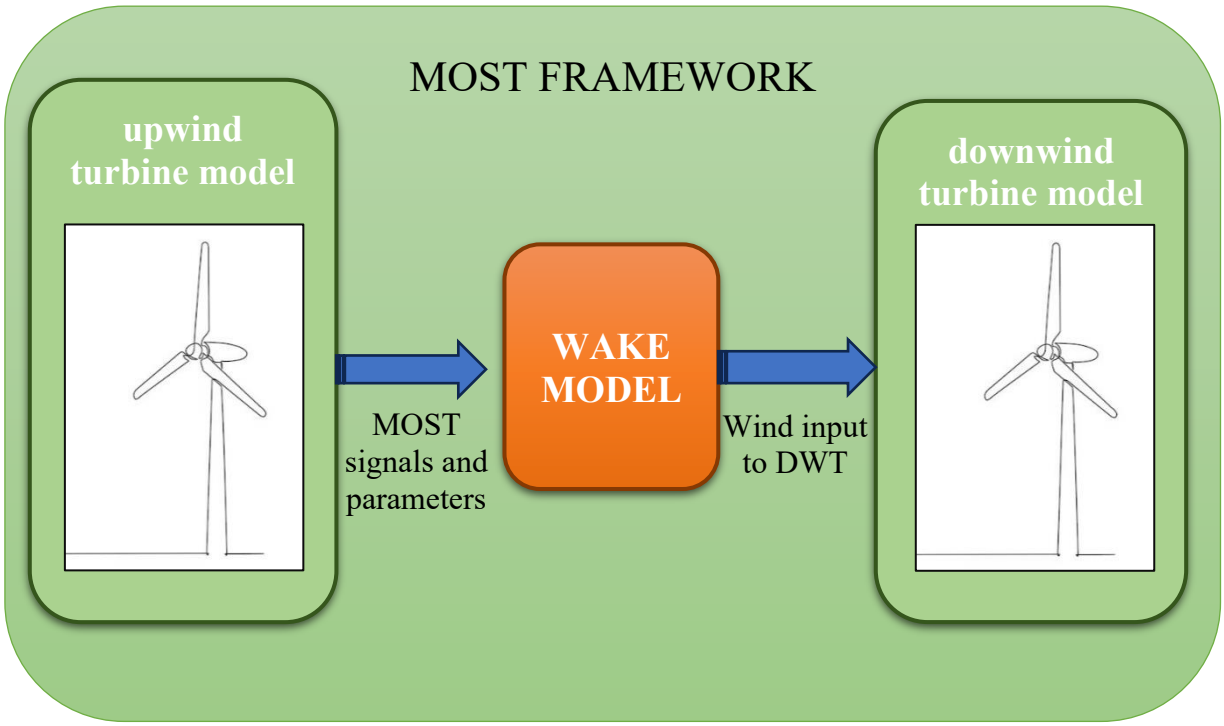

Figure 19 - block representation of the MOST framework embedded with the wake model

The implementation process begins with the generation of the wake signal, followed by its processing to ensure compatibility within the MOST environment, and ultimately its interpretation by the downwind turbine model.

Accordingly, this chapter will be divided into two main sections:

- Wake Generation module: This section will detail the implementation of the FLORIDyn code within the MOST framework for the purpose of generating the wake signal, with a focus on how the dynamic wake model was coupled with MOST inputs.

- Wake Processing module: This section will describe how the wake signal was processed to ensure correct interpretation by the downwind turbine block. Particular attention will be given to signal conditioning and data formatting in order to accurately reflect the physical interactions between the wake and the downwind turbine.

The following image is a scheme that represents all the features of the wake model. Each feature will be described in detail in the next sections.

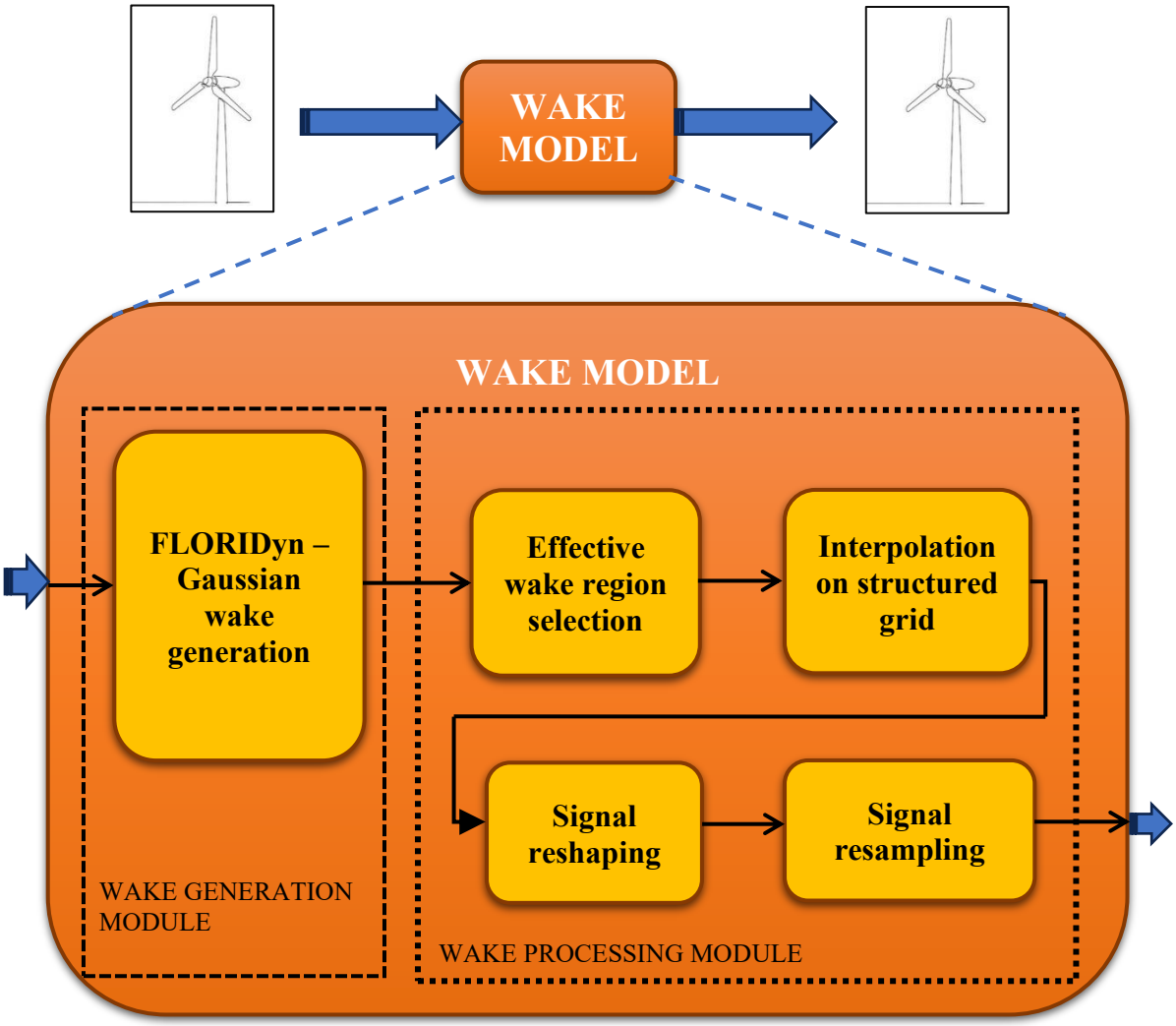

Figure 20 - block representation of the wake model, with its various functions. To better explain how the model works, the functions are split in two groups, the wake generation module and the wake processing module, highlighted by black dotted squares.

4.2 Wake Generation Module

4.2.1 Model simplifications

First, to implement FLORIDyn into MOST, some simplifications have been made, which will be corrected in future work. These simplifications include:

- Two turbines instead of multiple: though FLORIdyn is capable of simulating multiple turbines, in the present work the model will be implemented in MOST in the case of two turbines, aligned on the stream direction, leaving to future work the adaptation to multiple turbines.
- Wake combination model: as previously said in chapter 2, a combination model accounts for wake interaction. Since the focus of this thesis is to analyse the effects of the wake on the downwind turbine, the combination model has not been implemented.
- Shear effect: the incoming wind and wake field, due to the combined effect of ground surface roughness and atmospheric stability, should have a vertical gradient in stream velocity originally modelled in FLORIDyn with a power low. Since this thesis doesn't focus on obtaining accurate quantitative results, this effect will be neglected mainly for visualization purposes and to obtain a clear understanding of the model workings.
- Control algorithm: FLORIDyn does have different types of control strategies, but these will not be implemented in the present work. The yaw angle of the turbine upstream will be directly imposed by the user.

4.2.2 FLORIDyn into MATLAB function block

Since the MATLAB code implementing FLORIDyn is structured as a main script that sequentially calls a set of functions, the first step toward integrating this system into the Simulink environment of MOST involves creating a single MATLAB Function block, storing all the FLORIDyn functionalities.

The first key aspect to consider is that the function must retain memory of the variable states from the previous time step. This continuity is essential, as it is the basis upon which the wake can be generated and through which dynamic variations can be propagated over time.

To enable this, the data structures responsible for storing the positions of the observation points (OPs), their associated physical properties, the characteristics of the chains, the turbulence parameters, and the simulation settings must all be declared as persistent variables. This ensures

that their state is preserved across time steps, allowing for consistent and accurate temporal evolution throughout the simulation.

Secondly, it is useful to ensure that the function's output, specifically the spatial distribution of the observation points, each with its corresponding velocity vector, maintains a fixed size once the total simulation time is defined. This constraint enables the output to be handled as a fixed-size data structure, which significantly improves the post-processing workflow.

The third important aspect to consider is the sample time of the function. In the current simulation framework, the Simulink model operates with a base simulation time step of 0.01 seconds. However, the implemented wake model is not intended to provide a fully detailed or high-resolution representation of wake dynamics. Given this, to reduce computational load and overall simulation time without significantly compromising the quality of the results, the wake generation and processing blocks are assigned a coarser sample time, on the order of 1 second.

4.2.3 Coupling with MOST inputs

In order to illustrate the integration between the Wake Generation Module and the MOST framework, the following Simulink representation is presented:

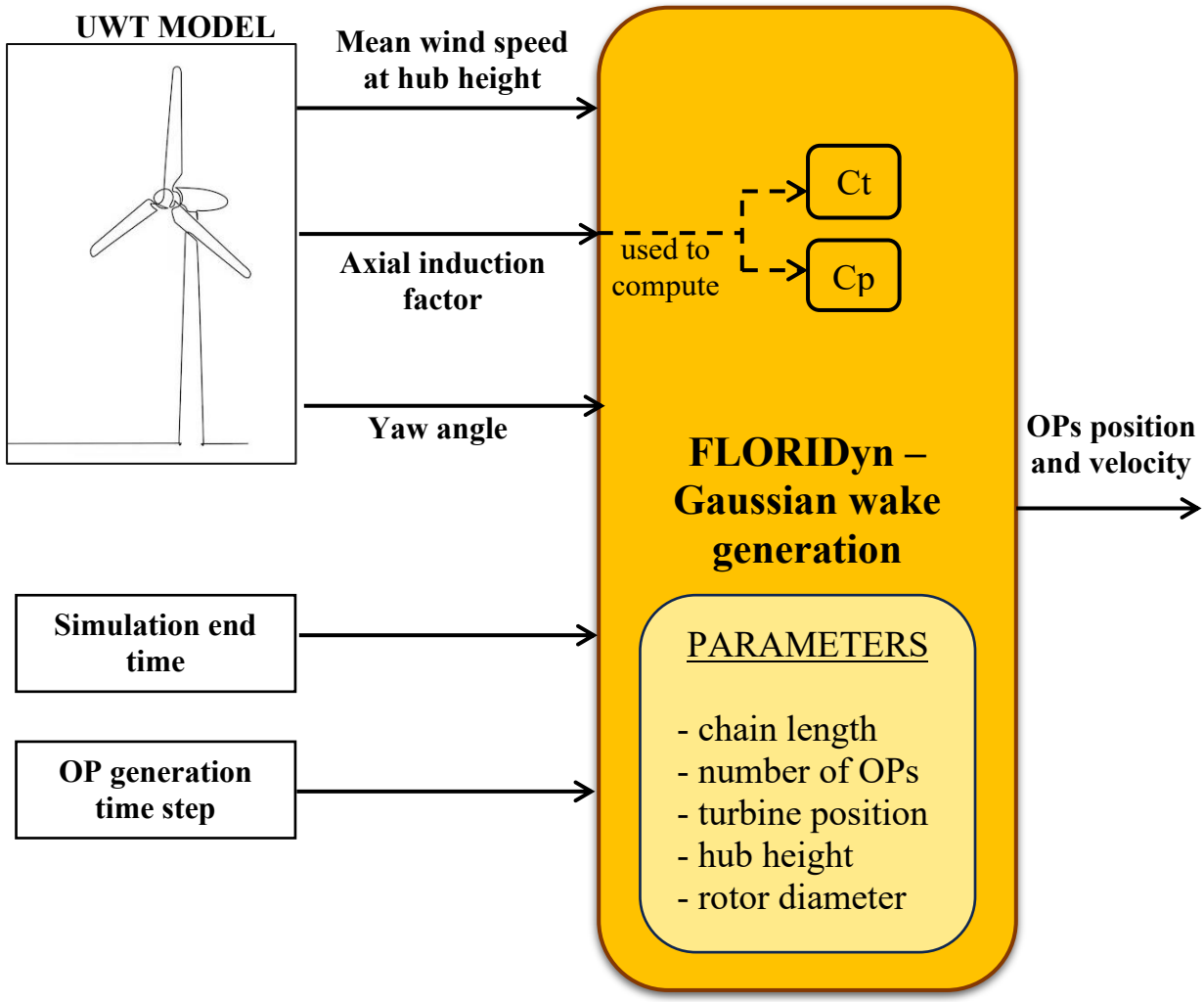

Figure 21- schematic block representation of the input/output signals of the function implementing FLORIDyn in MOST

As can be seen in Figure 21, the configuration of the wake model within the MOST framework requires the set of parameters listed and briefly described below:

- Turbine Position, Hub Height, and Rotor Diameter: Although not explicitly provided as inputs to the model interface, these values are defined internally as parameters within the function.
- OP generation Time Step: As previously discussed, the wake generation function operates with a coarser sample time compared to the base Simulink model. Specifically,

the wake-related blocks are assigned a time step equal to 100 times that of the main simulation loop.

- Simulation End Time: The total simulation time. Together with the time step, it determines the characteristics of the "chains", which are data structures that store and manage the temporal evolution of the observation points (OPs).
- Mean wind speed at hub height: The wind speed used as input of the wake model is the mean wind velocity evaluated at hub height. This is then split into magnitude and angle relative to the coordinate system. The wind magnitude is obtained by combining the X and Y components of the wind vector. The wind angle is derived as the arctangent of the ratio between the y-component and the x-component.
- Yaw angle: The yaw angle defines the angular misalignment between the turbine rotor axis and the y direction. In the context of this thesis, no closed loop control implementing wake steering strategies[2] has been implemented. Therefore, the yaw angle is directly imposed to the turbines, by setting it within the Simulink model.
- Axial Induction Factor[3]: This parameter can be obtained from the Blade Element Momentum (BEM) code of MOST that calculates the load on the blades. Specifically, it can be computed by averaging the local induction factors calculated at each blade segment (or node). It plays a key role in estimating the energy extracted by the rotor.
- Coefficient of Thrust (Ct): While not provided directly as an input to the wake model, it is computed using the axial induction factor with the simplified Glauert relation (1926) [22]:

$$C_t = 4a_{ax}(1 - a_{ax}\gamma) \tag{33}$$

Where a_{ax} indicates the axial induction factor, γ is the yaw angle and Ct is the coefficient of thrust.

- Coefficient of Power (Cp): The power coefficient is derived using the following relation:

$$C_p = 4a_{ax}(1 - a_{ax})^2 \tag{34}$$

[2] Wake steering is a control strategy used in wind farms to optimize power extraction. It is based on the assumption that wakes of upstream turbines have a negative effect on downstream machines, in terms of power generation. This control strategy aims to find a combination of the yaw angles of each turbine so that wake-turbine interaction is reduced.

[3] The axial induction factor determines the apparent wind approaching the rotor. It is defined as 1-u/V_0, where u is the velocity in the rotor plane and V_0 is the free wind speed

- Chain Length: The length of each chain is computed based on the total simulation time (End Time) and the time step used by the wake model.
- Number of Chains: This parameter defines the spatial resolution of the OP distribution across the rotor's cross-section. It is provided as an input parameter directly in the function code.

The code within the "FLORIDyn – Gaussian wake generation" block acquires at every time step the inputs listed above. With these it creates a new array of Observation Points at the rotor area and computes the new positions and velocities of the OPs already existing. These information are stored in the output signal "OPs position and velocity". In a more in-depths programming point of view, this signal is an *n* by 5 matrix, where *n* is the total number of OPs throughout the whole simulation and the 5 columns of each row store the x, y and z coordinates of each individual OP and the x and y components of the OP local velocity. The next paragraphs will explain in detail how this signal is elaborated in the processing module, and what each block does in order to transform the signal to a form that can be used in the BEM function of the downstream turbine.

4.3 Wake Processing Module

4.3.1 – Selection of the effective region of the wake

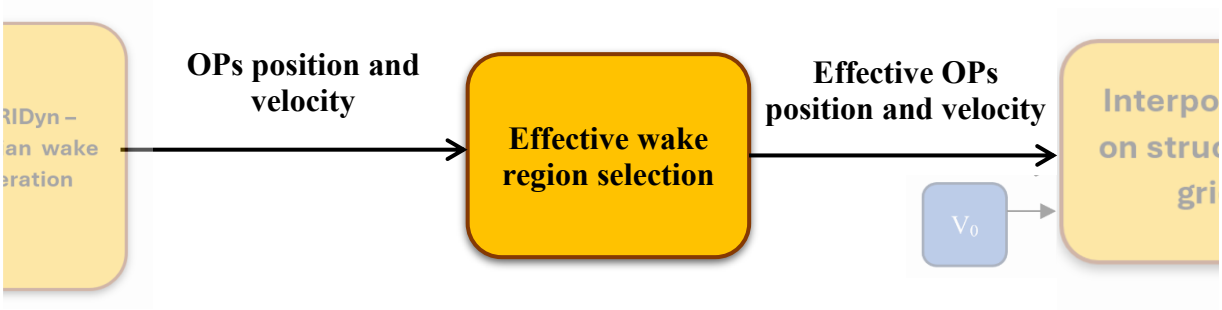

Figure 22 - input/output of the "Effective wake region selection" block. It is the first one of wake processing chain

Once the wake signal has been generated, it must be further processed to ensure correct interaction with the downwind turbine. The influence, in fact, is only perceived by the second turbine if the wake partially or fully intersects the wind field incident on that turbine.

The first step in this process involves selecting only those Observation Points (OPs), along with their associated velocity vectors, that are relevant to the downwind turbine. In other words, only

the portion of the wake that physically overlaps with the turbine's area of influence should be passed forward for analysis.

To achieve this, a spatial region is defined around the position of the second turbine. This region represents the zone within which OPs can interact with the rotor of the downwind turbine. For simplicity and computational efficiency, this region has been modelled as a right rectangular prism (a box-shaped volume) that encapsulates the turbine.

Only OPs located within this defined prism are retained for further processing, ensuring that the dynamic influence of the wake on the downwind turbine is computed only when the wake actually reaches and intersects its rotor-swept area.

This functionality is integrated in the block named “Effective wake region selection” as can be seen in the schematic representation of Figure 22. The output signal of this block is named “effective OPs position and velocity”. From a programming perspective, this signal is of the type variable size, which means that it does not have a pre allocated size. Its size can change throughout time steps, which is a necessity arising from the variable number of Ops entering the effective area in changing conditions of yaw and wind angle.

4.3.2 – Interpolation of OPs wind speed values on a structured grid

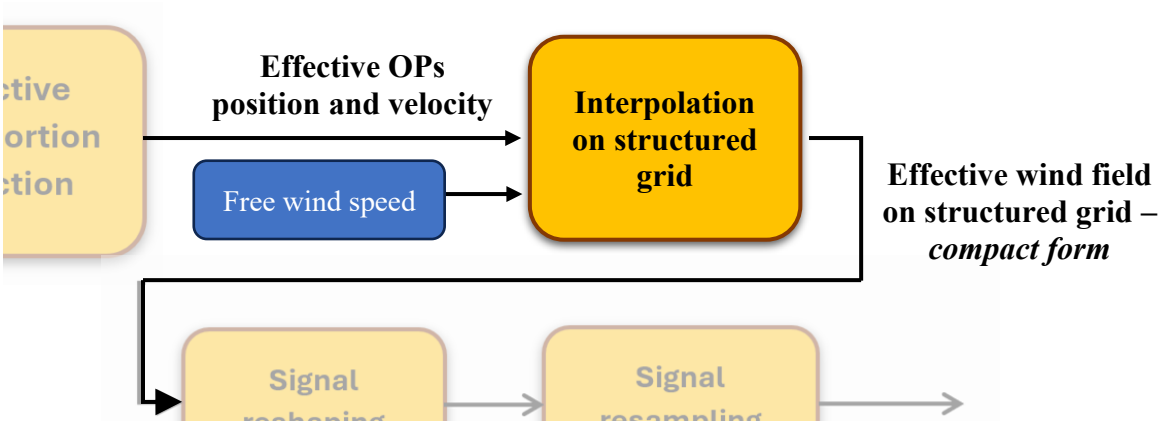

Figure 23 - input/output of the "Interpolation on structured grid" block. It is the second one of the wake processing chain

This paragraph focuses on the "interpolation on structured grid" block, as shown in the Simulink diagram above. This block is a Level-2 MATLAB S-Function, chosen instead of the MATLAB Function block for programming reasons. While the necessity of the wake selector, discussed

in the previous section, arises from the need to model a physical behaviour, the " interpolation on structured grid " block is introduced purely to address a programming requirement.
To understand its role, we must examine how the Beam Element Momentum (BEM) function of the downwind turbine processes the incoming wind signal. According to BEM theory [23] each turbine blade is discretized into a series of blade elements in order to compute local aerodynamic forces. In the corresponding Matlab function, each of these elements is represented with a node, and the input wind field is interpolated at the location of each node to determine the local inflow conditions. This interpolation is performed using Matlab's "interp3" function, which returns interpolated values for a function of three variables at specified query points using linear interpolation. However, interp3 only supports structured grids (i.e. the data points must lie on a regularly spaced 3D grid). This limitation gives rise to the need for the "interpolation on structured grid" block. The spatial distribution of the OPs, as generated by the wake model, is inherently unstructured. Therefore, to enable the downstream BEM function to properly interpret and interpolate the wind field, the velocity data must be re-mapped onto a structured grid. This preprocessing step ensures compatibility with the BEM module by producing a structured 3D field of velocity values that can be queried efficiently at the positions of the blade nodes using interp3. This is denoted as the "effective wind field on structured grid – compact form" signal in Figure 23. The "free wind speed" block is needed to impose free stream velocity when the wake does not yet interfere with the downwind turbine or to imparts free stream velocity in the portions of influence area not covered by the wake.

4.3.3 – Signal reshaping

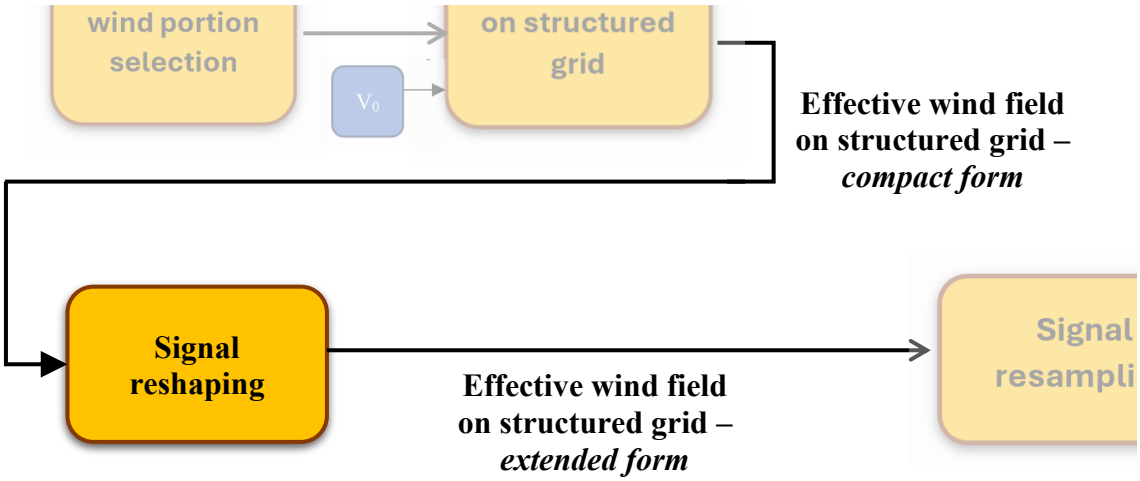

Figure 24 – input/output of the "Signal reshaping" block. It is the third one of the wake signal processing chain

This block also addresses a programming-level constraint rather than a physical modelling requirement. Specifically, the Level-2 MATLAB S-Function block, described in the previous section, does not support output signals with high-dimensional arrays, such as the multidimensional signal used to describe the wind (detailed in the subsection *"Coupling with MOST Inputs"*).

To work around this limitation, the "Interpolation on Structured Grid" block of Figure 23 includes a step that reformats the wind velocity signal using MATLAB's reshape function. At the end of the interpolation process, a dedicated reshape block, that can be seen in Figure 24, is used to restore the wind signal to its original multidimensional structure, allowing it to be correctly interpreted by the downstream modules.

4.3.4 – Resampling of the signal

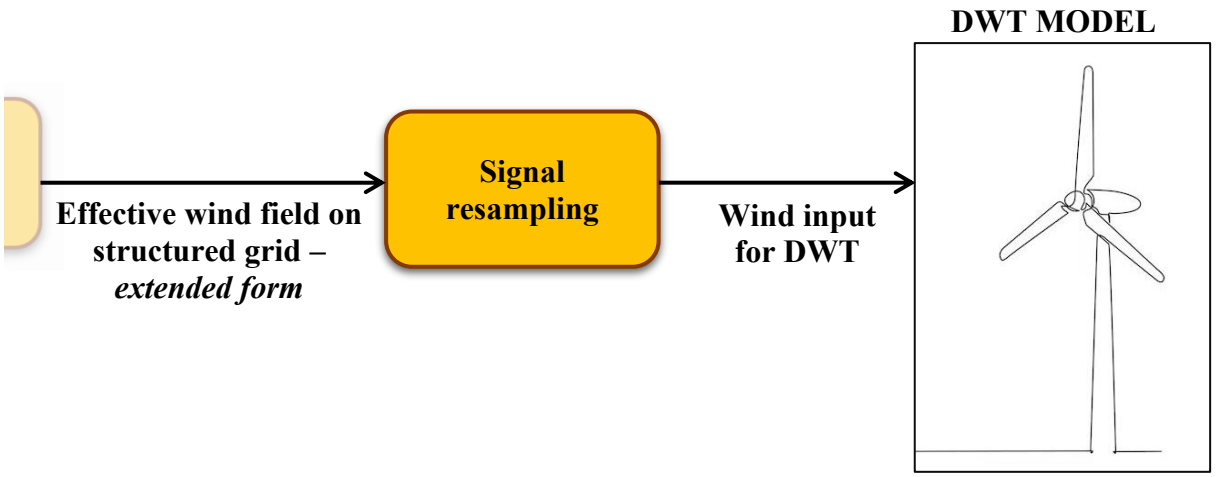

Figure 25 - input/output of the "Signal resampling" block. It is the last block of the processing chain. The output signal is ready to be processed by the downwind turbine model

The Zero-Order Hold (ZOH) function used in this model is a custom implementation, specifically developed to resample the wake signal and align its sampling time with the base simulation rate.

As previously discussed, the blocks responsible for wake generation and processing operate at a coarser sample time (on the order of 1 second), in order to reduce computational cost and improve simulation performance. However, since the base simulation time step in Simulink is set to 0.01 seconds, resampling is required to ensure compatibility between subsystems operating at different time resolutions.

To achieve this, a simple zero-order hold strategy was implemented. The custom function maintains the most recently received wake signal constant over time, until a new sample becomes available from the wake model. In practice, this means that the function holds the previous value and reuses it at each base time step, effectively producing a signal synchronized with the main simulation clock. The output of this function is the “wind input for DWT”, a signal ready to be correctly interpreted by the BEM function of the downwind turbine.

4.4 Insights into the wake visualization

The results obtained in the following chapter, through the simulation performed using the MOST framework and the FLORIDyn model, will be presented by means of several graphs. This section outlines the key features of these graphical representations, in order to improve their readability and to clarify the origin and meaning of the data they display. By providing this overview, the aim to ensure a correct interpretation of the upcoming results in chapter five and fully understand the modelling assumptions and simulation parameters from which they are derived.

4.4.1 – Insights into the wake visualization: OP 3D plot

The first graph illustrates the spatial distribution of the observation points (OPs), which are depicted as individual dots. The color of each dot corresponds to the magnitude of the velocity associated with that specific OP. Wind turbines are schematically represented by black circles, each denoting the rotor swept area. This visualization is intended to provide a comprehensive overview of the system's dynamics and overall operation. The OPs are transported downstream, carrying with them the flow characteristics inherited at the moment of their generation near the upwind rotor. This approach allows for a clear depiction of how wake effects and flow properties evolve spatially.

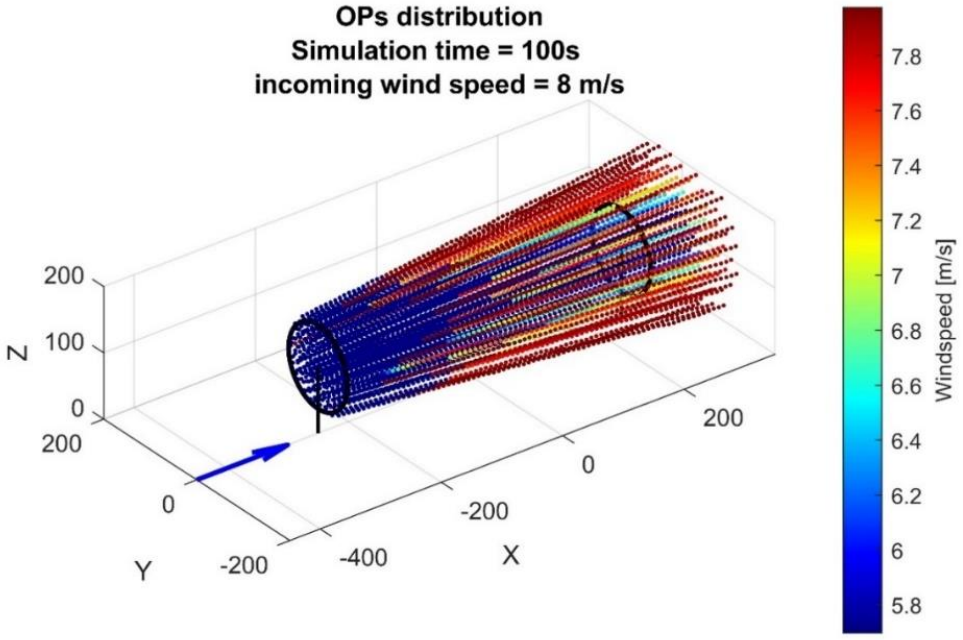

Figure 26 – first example of the plotting capabilities of the model. In this case the three-dimensional OPs distribution in terms of position and velocity is plotted

4.4.2 – Insights into the wake visualization: 2D wake contour

The information stored by the observation points (OPs) can also be interpolated onto structured grids, allowing for an approximate reconstruction of the velocity magnitude distribution. This post-processing technique enables the generation of continuous fields from discrete OP data, facilitating a more intuitive and visually interpretable representation of the flow characteristics. The accuracy of the interpolation, and, consequently, the quality of the reconstructed approximation, depends directly on the spatial density of the observation points (OPs). This applies both to their spacing within cross-sectional planes and to their distribution along the downwind direction. A finer and more homogeneous placement of OPs results in a higher-resolution approximation of the flow field, reducing interpolation errors. The following are two examples of plotting:

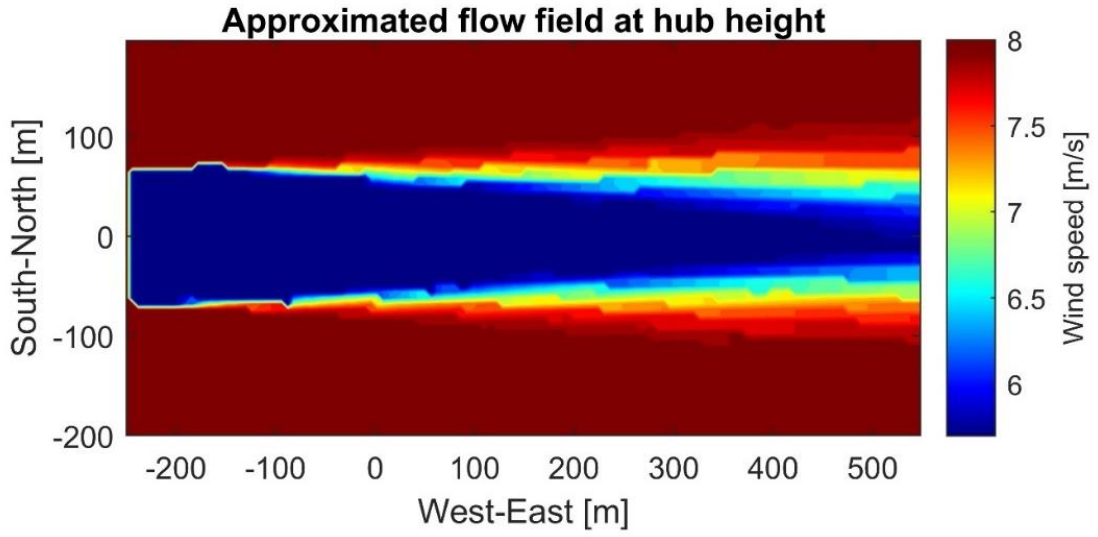

Figure 27 – second example of plotting capabilities: the OPs distribution is interpolated to give a contour of the flow field at hub height

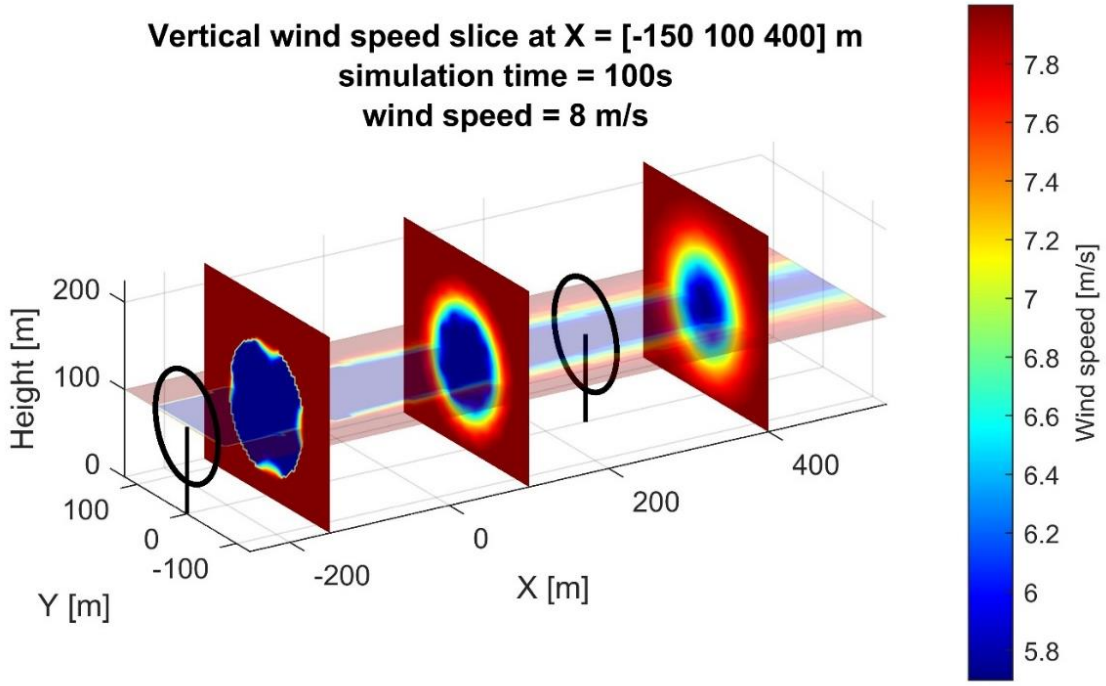

Figure 28 – third example of plotting capabilities: the OPs distribution is interpolated to give a contour of cross-sectional areas at different downstream positions

CHAPTER 5. RESULTS ANALYSIS

5.1 Case study setup and layout

The layout chosen for the testing of the model implemented consists of two turbines aligned along the rotation axis in non-yawed conditions.
The two wind turbines are composed of a floating platform of the spar type on which is mounted the NREL5MW [24] wind turbine. The assembly also include a catenary mooring system composed of three lines. The following image shows the wind turbine with its buoyancy system:

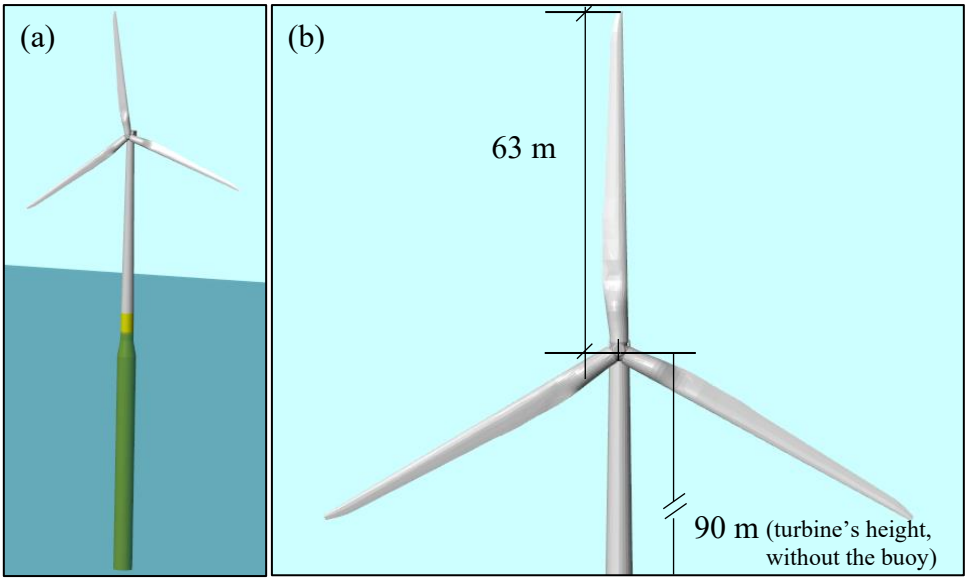

Figure 29 – in (a) the 5MW NREL Wind turbine with spar buoy, which is going to be used for the simulations. In (b) the most relevant dimensions of the turbine are noted. These images are one of MOST outputs.

The following images, Figure 30 and Figure 31, represent the selected configuration for the placement of the two wind turbines. As previously introduced, a configuration consisting of two turbines aligned in the downstream wind direction was selected, with a spacing of 500 meters between them. This simplified setup, involving only two turbines, was chosen to focus on the functionality of the wake model without introducing the additional complexity associated with a full wind farm layout. Furthermore, the inter-turbine spacing was deliberately set to be relatively short compared to typical values used in real-world wind farms, especially when measured against the actual rotor diameter (diameter of the swept area) of the turbines.

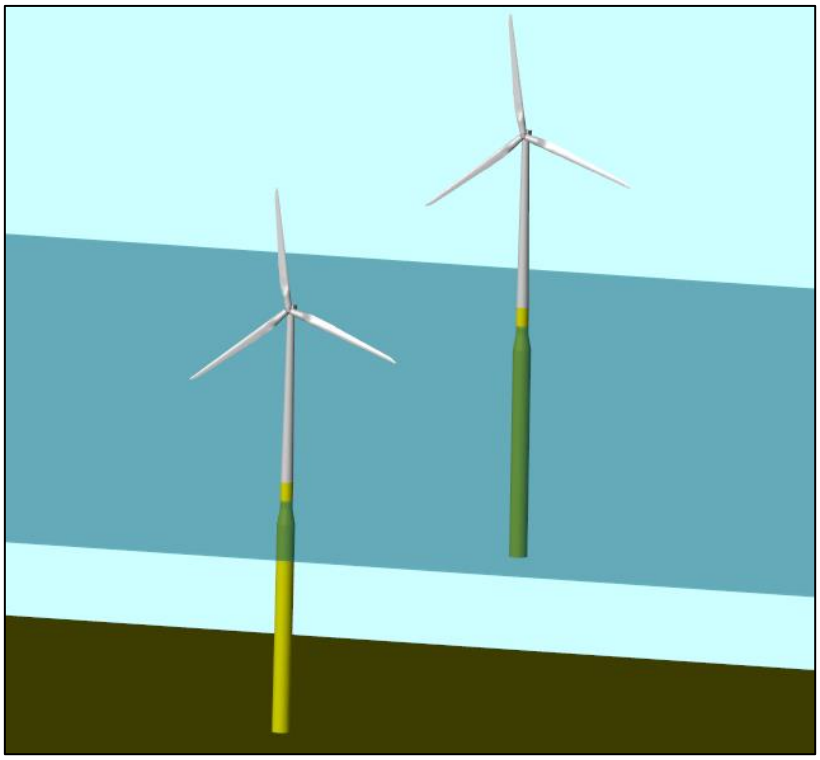

Figure 30 - Layout configuration of the two 5MW NREL wind turbines used in the simulations. This visualization is obtained with the direct input of the geometry of each component modelled in MOST.

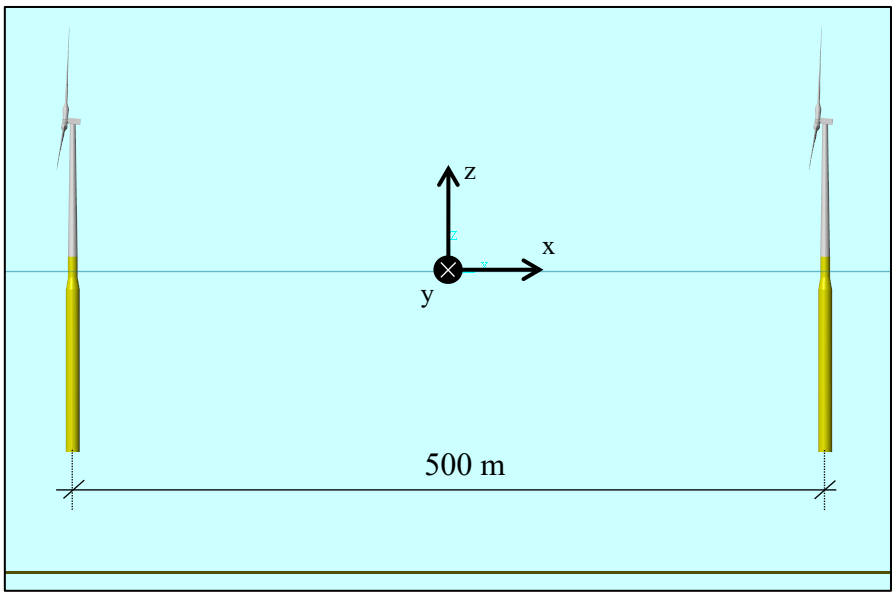

Figure 31 - Turbine distance in the streamwise direction

The chosen spacing was intentionally reduced for the following reasons. Given that this study is a qualitative analysis of the results derived by implementing a dynamic wake model, the focus was not on strict adherence to real-world spatial configurations. Instead, emphasis was placed on computational practicality and the clarity of result interpretation. Specifically:

1. Shorter inter-turbine distances allow the wake generated by the upstream turbine to reach the downstream turbine more quickly, resulting in reduced simulation times.
2. Tighter spacing facilitates clearer visualization of wake effects and system dynamics in plots and figures.
3. The power drop observed at the downstream turbine is more pronounced when the inter-turbine distance is reduced. This highlights the influence of the dynamic wake model more effectively, making the comparison between models more evident and meaningful.

The global reference system can be seen in Figure 31. It is a right-handed coordinate system located halfway between the two turbines and at sea level. Figure 32 illustrates the convention adopted for evaluating the incoming wind angles relative to the turbine, as well as the yaw angle definitions used throughout this work. To conclude this introductory part, it should be specified that a ROSCO (Reference Open-Source COntroller) controller is being used for both turbines in all the simulations, maximizing power in below rated conditions and regulating rotor speed in above-rated conditions. It consists of two methods of actuation: generator torque and collective blade pitch. The next section presents the results of the simulations carried out with the setup outlined in this paragraph.

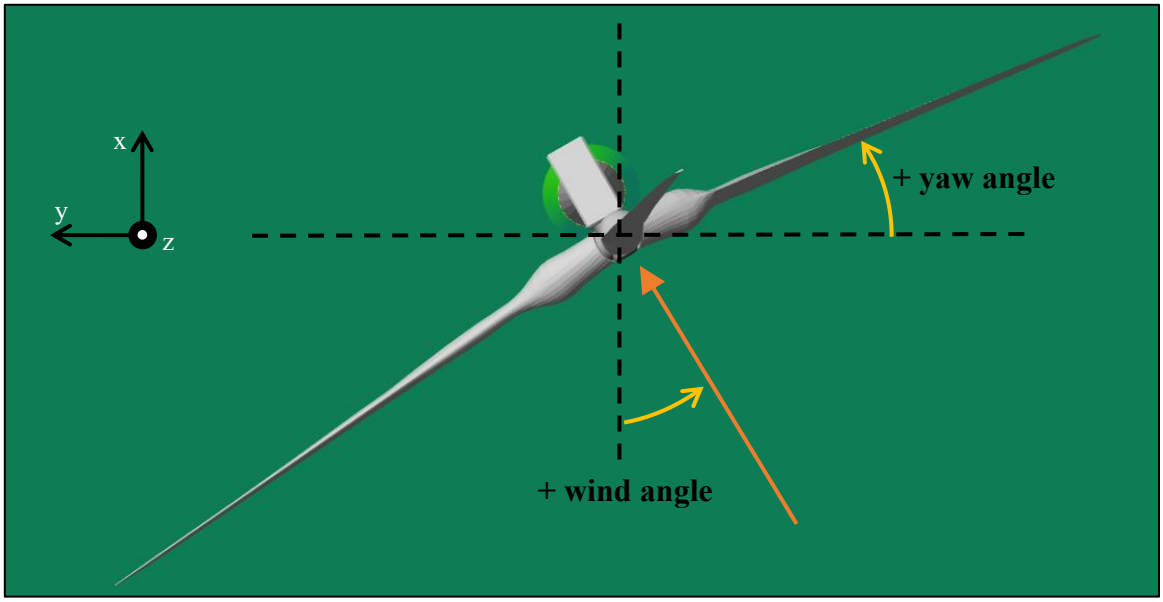

Figure 32 - x-y view of the wind angle and yaw angle convention

5.2 Simulation of the model during steady yaw and wind conditions

5.2.1 Simulation parameters

The turbine upwind and the turbine downwind will be respectively addressed as “wind turbine 1” and "wind turbine 2”. The simulations will be conducted with the following parameters:

Parameter	Value
Wind speed	Uniform, 8 m/s
Wind angle	0°
Simulation duration	200 s
Simulation Time-Step	0.01 s
Significant Wave Height	4 m
Number of OP chains[4]	100
Axial induction factor	0.1414
Wave Peak Period	6 s

Table 1 – Parameters of the steady-state simulation to retrieve the power generation

5.2.2 Power output analysis

Having implemented the wake model for the upwind turbine, the objective of this section is to show how the characteristics of the downwind turbine are influenced by such implementation. First, we address the power production, of which is presented the following graph:

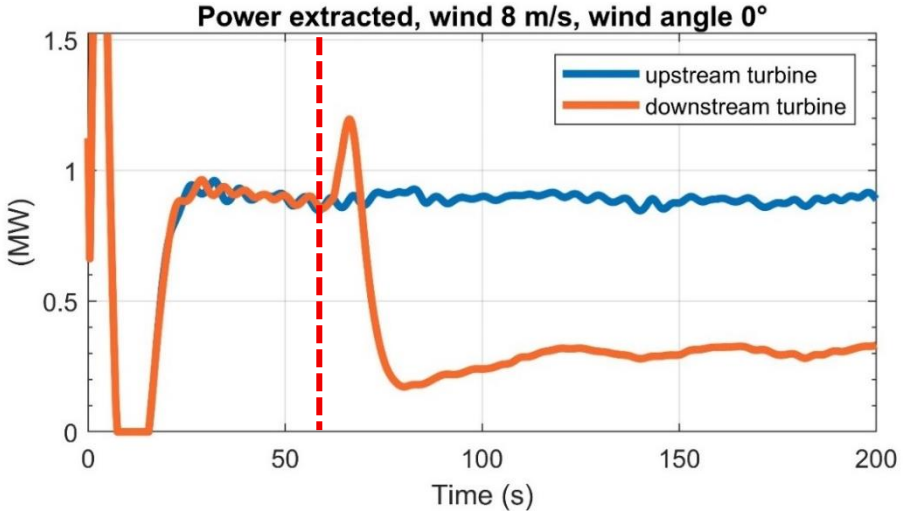

Figure 33 - Power generated over time in a non-yawed scenario. The red dashed line corresponds to the instants in which the wakes reaches the downwind turbine

[4] As specified in Chapter 3, a chain is a set of OPs that originate from the same relative coordinate on the rotor

As can be observed in Figure 33, when the wake enters the influence zone of the second turbine, its power experiences a significant drop. Since the downstream turbine is exposed to a flow field that has already been disturbed and decelerated by the wake of the first turbine, it is subjected to reduced aerodynamic forces. As a result, its rotational speed decreases, leading to a noticeable reduction in the power output.

Although the drop in the power output is amplified because of the reduced distance between the turbines, it is nonetheless clear the importance of wake models in farm simulations, where the wake effects can play a crucial role in the correct estimation of the global power extraction. Moreover, this first series of simulation results shows the peculiar aspect of this dynamical approach to wake modelling. The power drop occurs only after the wake has travelled its way through the inter-turbine distance, leading to a more realistic simulation. This will be more evident in following chapters, in which the model will be tested with dynamic changes in external conditions.

It is necessary to point out that:

- The discontinuity in the power graph occurring at the start of the simulation can be neglected, because it is due to non-physical aspects.
- The quick rise in power extracted by the second turbine that can be seen in Figure 33 and corresponds to the moment the wake enters the influence area can be due to the sudden transformation of the kinetic energy of the rotor into energy extracted by the generator.
- As will be later explained in more detail for the dynamic simulations, which will take into account time-varying wind conditions, the wake model module is not optimized to accept instantaneous and varying values of the axial induction factor for the calculation of the thrust and power coefficients at each time step. Therefore, a mean value has been used. This corresponds to the mean value across the rotor area, averaged over time, neglecting the transient.

Taking advantage of the dynamic FLORIDyn model, it will now be shown a time representation of the wake, through the spatial distribution of the Observation Points (OP). To obtain a signal more suited for the visualization, the simulation has been restarted with the sample time of the wake module further reduced to 4 seconds and the number of chains increased up to 300. But firstly, the power history will be plotted again, with time stamps indicating various instants of the simulation. By referring to these, it will facilitate the time representation of the wake.

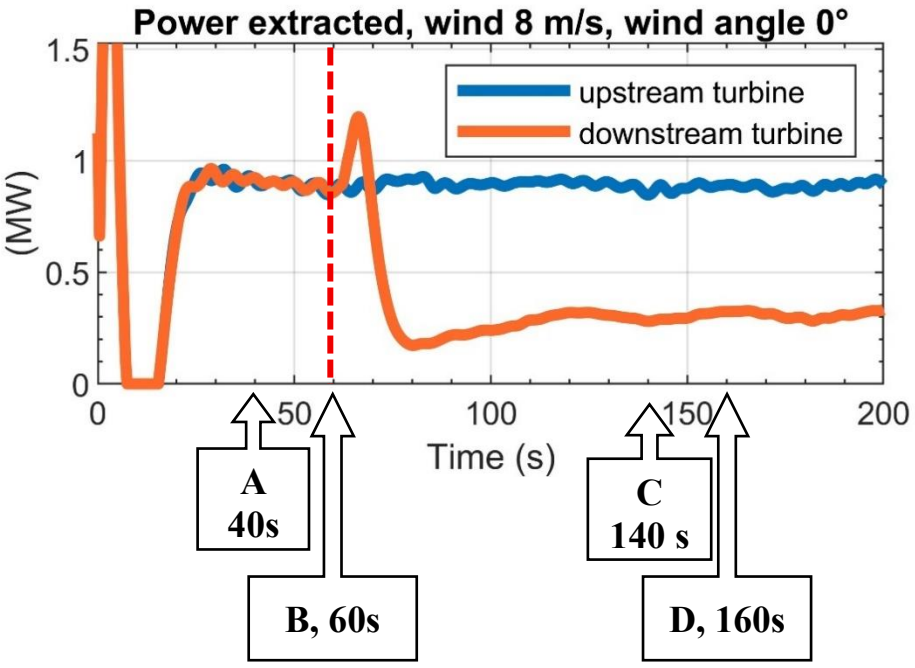

Figure 34 – Indexing of four instants in the power generation graph that will be used to show the wake evolution over time. The red dashed line corresponds to the instants in which the wakes reaches the downwind turbine

The fully developed wake field is shown in Figure 35. The underlying workings of the model are clearly illustrated: at each time step, an array of Observation Points (OPs) is generated and transported downstream with the free-stream wind velocity. This velocity is used as a practical means carry the OPs' information downstream. The actual local velocities are stored within each OP. These velocities are then visualized using a colorbar. From the graphs the physical modelling of the wake is also clear. It can be seen the evolution of the potential core of the wake (the uniform velocity zone extending behind the rotor and described in more detail in Chapter 2) and the wake velocity recovery to the free stream speed. In the next page, in Figure 36, the time evolution of the field will be displayed.

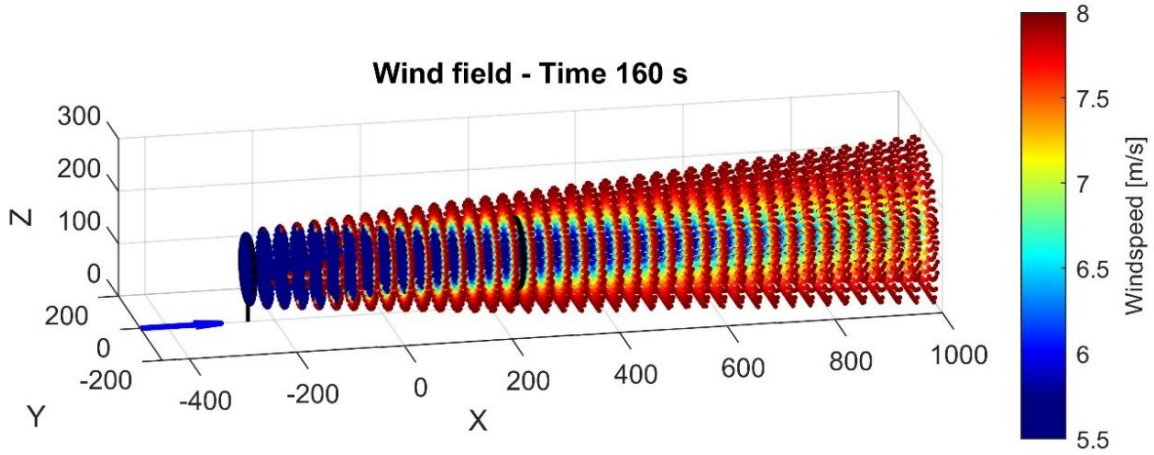

Figure 35 - wind field corresponding to point denoted by the letter D in the power graph of Figure 34

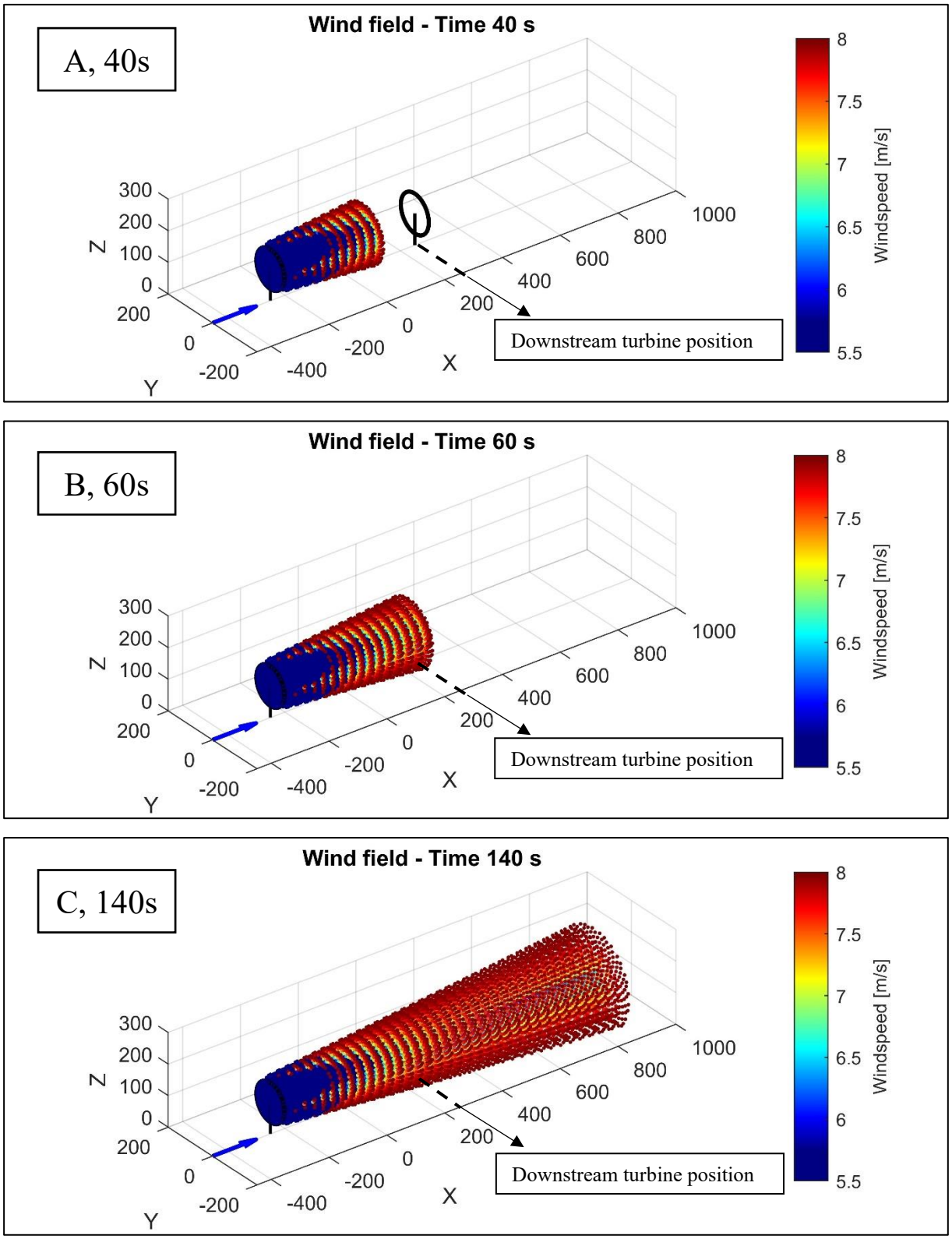

Figure 36 - evolution of the wind field behind the upstream turbine in steady state conditions. The figures correspond from up to bottom to the time instants denoted by letters A, B and C in Figure 34

5.2.3 Kinematic behaviour in steady-state wind conditions

Power extraction is the result of the interaction of the incoming wind with the rotor blades. It is therefore clear that a variation in power stems from the variation of the aerodynamic forces acting on the turbine, and consequently from the variation of the rotor's angular velocity. So, to fully understand the effects that the wake-turbine interaction has, one has to also analyse the kinematic and dynamic behaviour of the turbine. This can give insights into securing the turbine from fatigue damage.

For these reasons, the previous steady-state simulations have been repeated with a greater simulation time (as can be seen in Table 2), and the results in terms of turbine motion are presented in this section. In particular, Figure 37 illustrates the time evolution of the pitch angle for both UWT (Upstream Wind Turbine) and DWT (Downstream Wind Turbine).

Parameter	**Value**
Wind speed	Uniform, 8 m/s
Wind angle	0°
Simulation duration	1000 s
Number of OP chains	100
Wake module sample time	4 s

Table 2 - Parameters of the steady-state simulation to retrieve the kinematic and dynamic behaviour

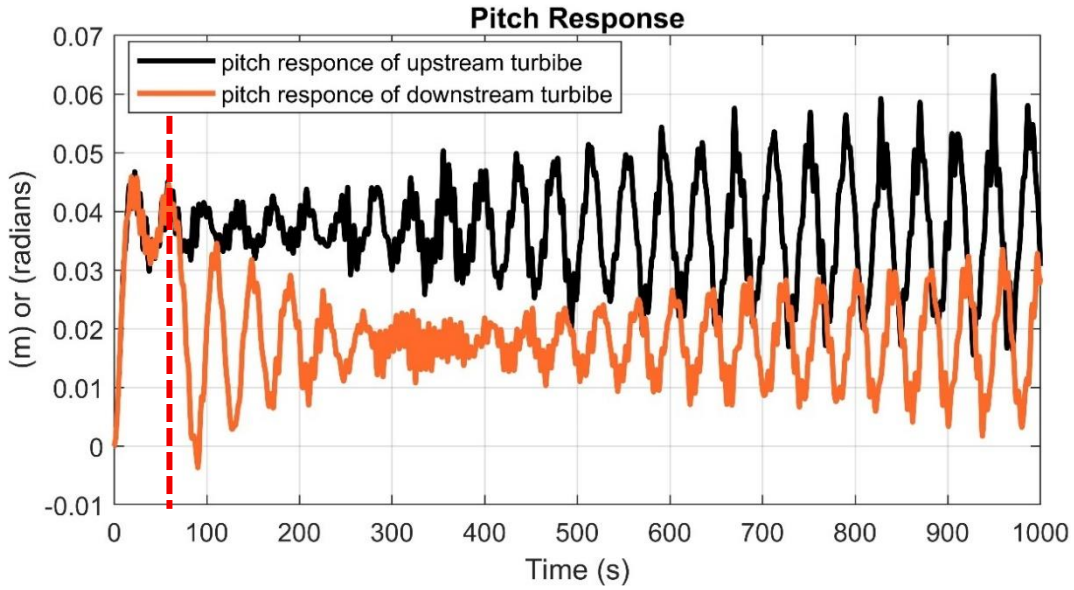

Figure 37 - pitch response of the upwind turbine (black) and the downwind turbine (orange) in the non-yawed case. The red dashed line indicates the moment the wake arrives in the downwind turbine influence area

From the analysis of Figure 37, it can be observed that when the wake reaches the downstream wind turbine (DWT), the pitch angle exhibits a lower mean value. Additionally, the amplitude of the oscillation appears to decrease. Moreover, the signal seems to result from the superposition of multiple frequency components. A greater simulation end time has been used in the current section, to capture lower frequencies with larger oscillation period. A proper characterization of these frequencies would require a spectral analysis, which is outside the scope of this thesis.
What can be stated is that, as a consequence of the reduced wind speed within the wake region, the pitch response of the downstream wind turbine tends to assume a lower mean value. Nevertheless, this value appears to remain in the same order of magnitude of the former value.

5.2.4 Dynamic behaviour

As previously introduced, understanding the load history of the blades is crucial to ensure structural integrity during different operating conditions, both in design phase and during functioning. Low computational cost tools like the one being used are useful to give first results, that can help to identify potential critical conditions. For these reasons, the dynamic effect of the wake on the downwind turbine will be analysed. This section presents graphs illustrating the evolution of the aerodynamic loads on both turbines. These loads are broken down into their Y and X components to provide a more comprehensive understanding of the loading conditions. Only the first 200 seconds of the simulation will be shown, to make the visualization clearer. Analysing Figures 38 and 39 presented, it can be observed that the main effect registered is a decrease in the magnitude of the aerodynamic forces acting both in the streamwise and in the spanwise directions. Once again, a frequency spectrum analysis would be required to determine whether the wake has an effect also on the frequency of the forces.
It should be paid attention to Figure 39, where the trend of the forces acting on the downwind turbine's blades seems to increase, but this interpretation would not be correct. In fact, the absolute value of the load is decreasing, and the trend of the graph is due to the coordinate system used.
In conclusion, the global effect of the wake over the loads perceived by the downwind turbine is a general decrease in their magnitude. However, the reader is reminded that this cannot be taken as a general conclusion. The reasons are mainly two and they will be explained shortly.

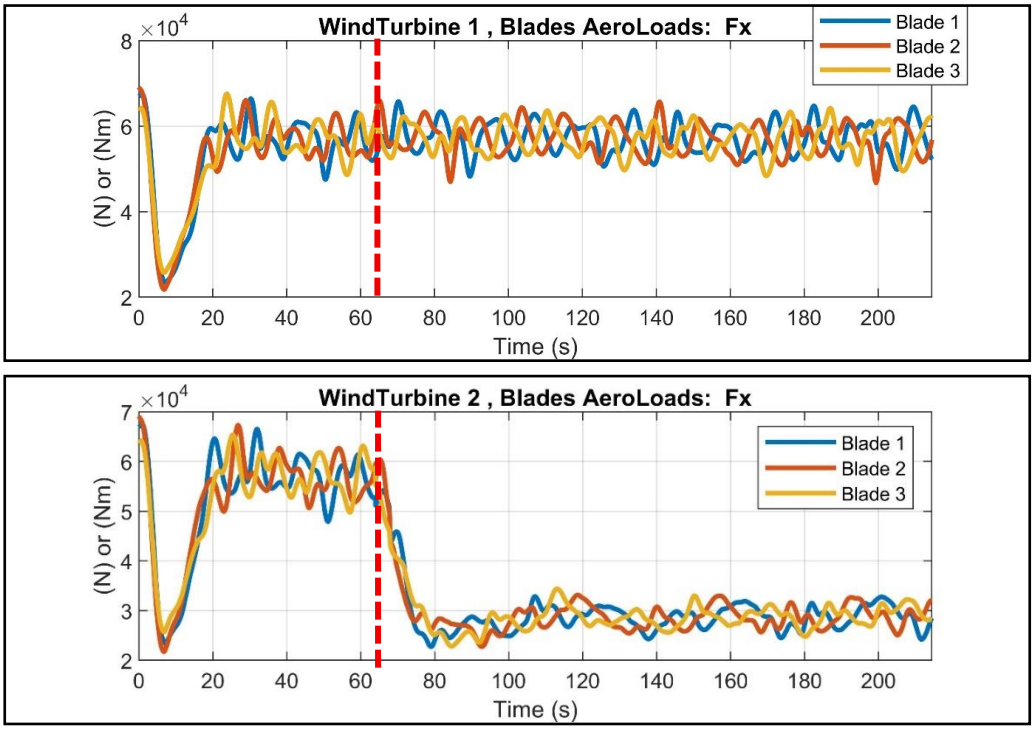

Figure 39 - time history of the x component of the aerodynamic force acting on the three blades. The dashed red line represents the moment in which the wake of the upwind turbine reaches the downwind turbine

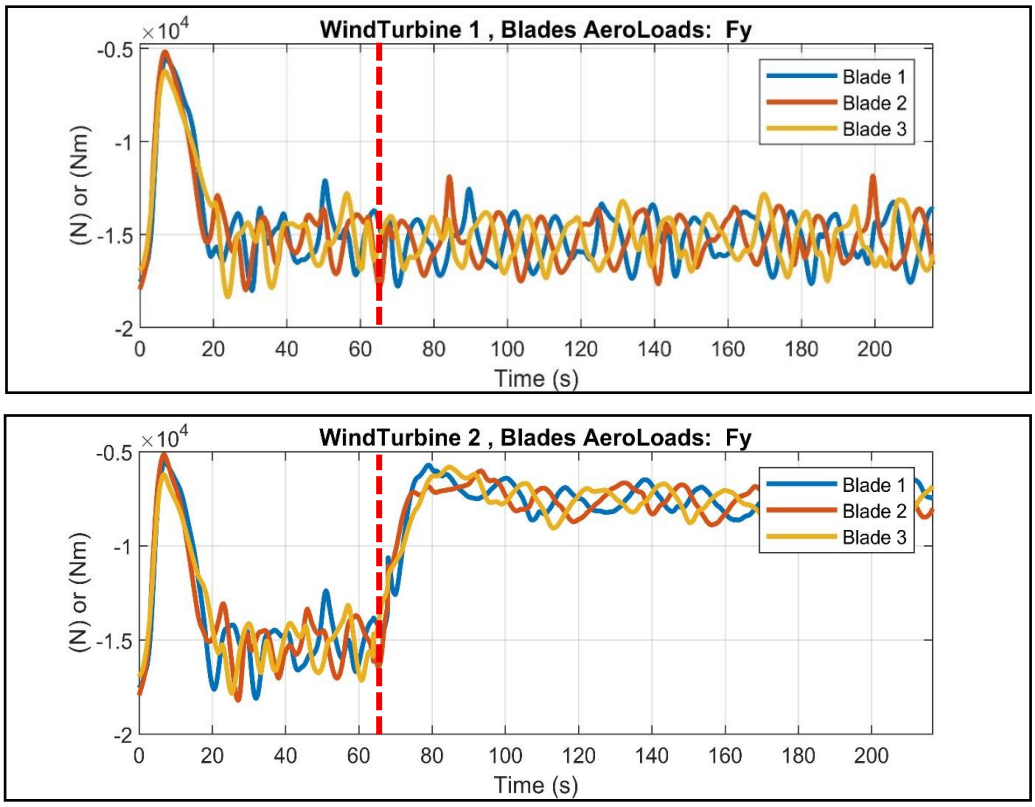

Figure 38 - time history of the y component of the aerodynamic force acting on the three blades. The dashed red line represents the moment in which the wake of the upwind turbine reaches the downwind turbine

The first reason why general conclusions cannot be drawn from the analysis of the presented graphs is that the model has several limitations:

- The turbulence model adopted for the wake representation is relatively simple.
- The influence of the ground, particularly in terms of the shear layer, has been neglected.
- The case study considers only two turbines, which is inherently limiting. In a real wind farm, the cumulative effect of multiple upstream wakes would need to be considered.
- The upwind turbine is subjected to a steady, non-turbulent inflow, which does not reflect realistic atmospheric conditions.

The second reason why these results should be contextualized is the experimental evidence. It is documented that in actual wind farms, the downstream turbines, despite being exposed to a reduced wind speed, experiences higher fatigue loading due to the added turbulence originating from the wakes of upstream turbines [25]. In this context, control strategies such as wake steering, which are typically employed to optimize overall power extraction across the wind farm, can also be used to manage fatigue loads across individual turbines [26].

For these reasons, to obtain more accurate results, the gap between this model and high-fidelity simulation tools must be bridged. Further dynamic analysis is deferred to future studies, where the current model approximations will be addressed and refined.

5.3 Simulation of the model during dynamic wind conditions

In the past section the model has been tested with a steady-state wind field acting on both turbines. Since the model has the capability to also address changing conditions, modelling the propagation of turbine states through the wake, in the current section will be analysed the results obtained from simulations involving dynamic wind inflow conditions acting on the two turbines. Specifically, a wind angle sweep will be performed, ranging from +30 degrees to -30 degrees, in accordance with the angle measurement convention introduced at the beginning of this chapter. This analysis aims to assess how variations in wind direction influence the aerodynamic interaction between the turbines and the resulting wake dynamics.

Before proceeding it should be pointed out that, since the wake model module has not yet been optimized to accept time-varying values of the axial induction factor for the calculation of the thrust and power coefficients at each time step, a single constant axial induction factor was selected for the simulation carried out. To obtain this value a preliminary simulation has been performed, with the wake model deactivated and wind direction parallel to the x axis. This preliminary simulation has been used to extract at every time step the axial induction factor from the code implementing the Beam Element Momentum (BEM) as the mean value over the entire rotor area of the node-specific axial induction factors. The resulting time series has been averaged excluding the first 120 seconds to eliminate the effects of the transient phase. The mean value obtained has been used as a fixed input for the wake model in the main simulation. Assuming a constant axial induction factor therefore introduces a degree of quantitative inaccuracy, especially as the yaw angle increases. In fact, when there is a misalignment between the rotor axis and the wind direction, the axial induction factor decreases. This reflects the reduced ability of the turbine to extract kinetic energy from the incoming flow. However, the objective of this section is to demonstrate the qualitative capabilities of the wake model, specifically, its applicability in wake steering strategies aimed at power optimization.

As long as the overall shape of the power curve is reasonably preserved, it is considered acceptable, for the purposes of this analysis, to assume a constant axial induction factor with varying wind direction. A more accurate modelling of its variation is left as a subject for future work.

The parameters used in the simulation are listed in Table 3. In Figure 40 it is showed the graph of the power generated at every time step.

Parameter	Value
Wind speed	Uniform, 8 m/s
Wind angle sweep	+30° -> -30°
Simulation duration	200 s
Number of OP chains	100
Axial induction factor	0.1414
Wake module sample time	1 s
Yaw angle	0°

Table 3 - Parameters of unsteady simulation, under time-varying wind direction

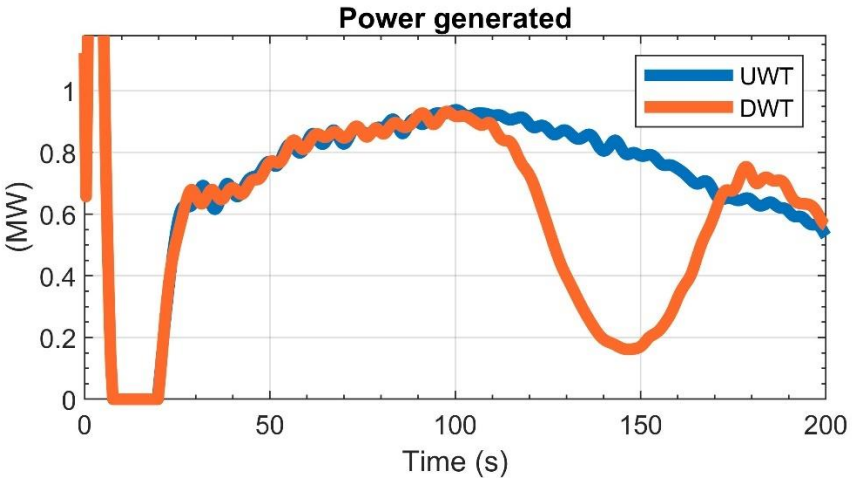

Figure 40 - power generated over time by the two turbines in the case of a linearly varying wind direction from +30° to -30°

Firstly, it should be pointed out that the first seconds of the power trend in Figure 40 should not be taken into account, because they have no physical meaning. That said, by analysing Figure 40, it can clearly be seen how the wind direction influences the power extraction. The power generated by the upwind turbine, denoted by the blue signal, experiences an increase as the wind direction linearly diminishes from 30° to 0°. The latter corresponds to the alignment between the wind direction and rotor axis. It is exactly in this configuration that the energy extraction reaches its maximum. When the wind direction angle then increases in negative values, ranging from 0° to -30°, the power generated experiences a decline.

Now, considering the downwind turbine, which signal is represented in orange, it can be seen that the power generated follows closely the one of the upwind turbine. That is clear, considering that during the first part of the simulation both turbines are subjected to the same wind input. When the wake of the upwind turbine reaches the downwind turbine, the power drops, due to the diminished velocity of the wind. Only after the wake exits the influence zone around the swept area of the DWT, its power starts to rise again.

In Figure 41 the power trend is plotted against a representation of the wake, through the OP's spatial distribution in the x – y plane. Three time instants are displayed and the impact of the wake on the downstream turbine in terms of power loss becomes evident.

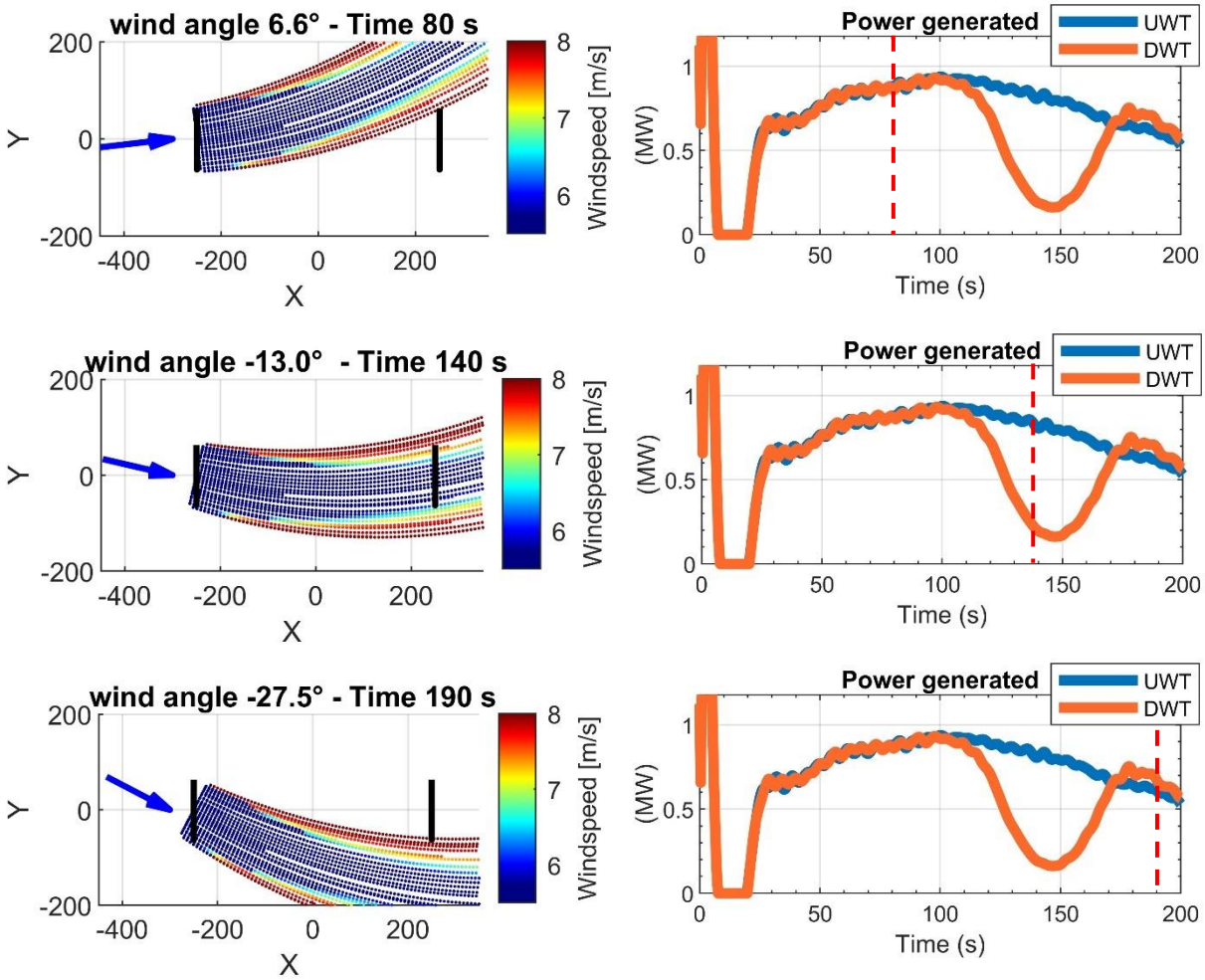

Figure 41 - the wake evolution is plotted against power extraction. The wake plot instants correspond to the red dashed lines in the power graph. It can be seen that the negative wake influence on the downwind turbine persists only when the wake enters the downstream turbine swept area.

The results highlight the model's capability to dynamically capture changes in external conditions, in this case variations in wind direction.

This demonstrates that the modelling approach offered by FLORIDyn, coupled with the MOST framework, enables to reproduce the dynamic response of the system to time-varying conditions. This reinforces the advantages of employing accurate dynamic wake models, which allow for realistic simulations of transient behaviour in both turbine performance and flow conditions. Such modelling capabilities are crucial for improving wind farm layout optimization algorithms, as well as for enabling the implementation of closed-loop control strategies, which could rely on a realistic, time-resolved representation of wake effects and their influence on farm dynamics.

CONCLUSIONS

In this work, the procedure for implementing the FLORIDyn model within the MOST environment has been presented, along with a set of simulation results under both steady-state and dynamic conditions. The unique features of the FLORIDyn model were discussed in detail and analysed in relation to the implementation process.

The study demonstrated that incorporating wake modelling is essential when addressing wind farm layout design and control strategy development. In particular, dynamic wake models such as FLORIDyn, which enable the simulation of the propagation of time-varying turbine and wind states within the wake, can serve as powerful tools to support the development of more advanced and optimized layout and control methodologies.

While the current implementation yields satisfactory qualitative results, several aspects require improvement in order to enable full validation of the model against high-fidelity simulation tools. Future work can be structured along three main directions:

Model optimization and validation against high-fidelity simulations

The priority is refining the current implementation of the FLORIDyn model to bridge the gap between its predictions and those produced by high-fidelity simulation tools, with the goal of validating the model. In this regard, several key areas of uncertainty and improvement have been identified:

- Turbulent inflow conditions: Currently, the implemented wake model is limited to cases with laminar inflow. An essential development step is to enable the use of the wake model under turbulent inflow conditions, as defined in MOST.
- Velocity component limitations: At present, FLORIDyn only accounts for velocity components in the y-x plane. To enhance the physical realism of the model, a revised formulation should be introduced to also account for velocity components along the z-direction.
- Shear layer modelling: Although FLORIDyn includes a power-law formulation to model the wind shear layer near the ground, this feature was intentionally excluded in the present work to improve the clarity of visualization plots. For the model to provide quantitative results, rather than solely qualitative trends, it will be necessary to integrate shear layer modelling into the coupled FLORIDyn–MOST framework.

Extension of wake modelling to multi-turbine wind farms

The second area of development concerns the extension of the model to simulate wake generation and propagation within a complete wind farm. This requires the integration of a wake interaction model capable of capturing the mutual influences among multiple turbines. To do so, the existing interaction framework between MOST and FLORIDyn will need to be revised.

Integration of wake-aware control strategies

The third direction involves modifying MOST's current control algorithm to account for wake effects. In particular, this would include the implementation of wake steering strategies aimed at maximizing total farm power output. As briefly discussed in this thesis, wake steering involves determining an optimal combination of yaw angles across turbines to minimize the negative influence of wakes on downstream turbines.

Nevertheless, FLORIDyn represents a valuable addition to the MOST environment, and the results obtained so far are promising. The integrated tool is particularly well-suited for supporting the optimization of wind farm layout design algorithms, and, thanks to FLORIDyn's ability to handle dynamic operating conditions, as demonstrated in the results chapter, it also holds significant potential for enhancing control strategies. In particular, it could be used in the development of closed-loop control designs that explicitly account for wake dynamic effects, leading to more efficient and adaptive wind farm operation.

BIBLIOGRAPHY

[1] MOREnergy Lab. MOST User Guide. Tech. rep. Politecnico di Torino, 2024. url: https ://github.com/MOREnergylab/MOST/blob / master/Docs/MOST_GUIDE.pdf.

[2] NREL. (2020). OpenFAST v2.1: User's guide and theory manual (Technical Report No. NREL/TP-5000-75811). National Renewable Energy Laboratory. https://doi.org/10.2172/1600030.

[3] Porté-Agel, F.; Bastankhah,M.; Shamsoddin, S.Wind-Turbine andWind-Farm Flows: A Review; Springer: Dordrecht, The Netherlands, 2020; Volume 174, ISBN 1054601900473.

[4] Jensen, N. O. (1983). A note on wind generator interaction (Risø-M-2411). Risø National Laboratory.

[5] Vermeulen P., Builtjes, P., Dekker, J. and van Bueren, G.L. (1979): An experimental study of the wake behind a full scale vertical-axis wind turbine. TNO-report, No. 79-06118. Laan van Westenenk 501, Apeldoorn, The Netherlands.

[6] P. M. O. Gebraad, F. Teeuwisse, J. van Wingerden, P. A. Fleming, S. D. Ruben, J. R. Marden, and L. Y. Pao. A data-driven model for wind plant power optimization by yaw control. In 2014 American Control Conference, 2014. doi:10.1109/ACC.20.

[7] Jiménez Á., Crespo A., and Migoya E., Application of a les technique to characterize the wake deflection of a wind turbine in yaw. Wind Energy, 13(6):559–572, 2010. doi: https://doi.org/10.1002/we.380. URL https://onlinelibrary.wiley.com/doi/abs/10.1002/w.

[8] Bastankhah, M. and Porté-Agel, F.: Experimental and Theoretical Study of Wind Turbine Wakes in Yawed Conditions, J. Fluid Mech., 806, 506–541, https://doi.org/10.1017/jfm.2016.595, 2016.

[9] Crespo, A. and Hernández, J.: Turbulence characteristics in wind turbine wakes, J. Wind Eng. Indust. Aerodynam., 61, 71–85, https://doi.org/10.1016/0167-6105(95)00033-X, 1996.

[10] ma, Yulong & Vasel-Be-Hagh, Ahmad. (2022). The Jensen wind farm parameterization. Wind Energy Science. 7. 2407-2431. 10.5194/wes-7-2407-2022.

[11] National Renewable Energy Laboratory (NREL). (2024). FLORIS v3.5.1 [Computer software]. https://github.com/NREL/floris.

[12] DTU Wind Energy. (2024). PyWake v2.5.0 [Computer software]. https://github.com/TUWien-PyWake/PyWake.

[13] M. Becker et al. “The revised FLORIDyn model: implementation of heterogeneous flow and the Gaussian wake”. In: Wind Energy Science 7.6 (2022), pp. 2163–2179. doi: 10.5194/wes-7-2163-2022.

[14] Grunnet, J. D., Soltani, M., Knudsen, T., Kragelund, M. N., and Bak, T.: Aeolus Toolbox for Dynamics Wind Farm Model, Simulation and Control, in: European Wind Energy Conference and Exhibition, EWEC 2010, 20–23 April 2010, Warsaw, Poland, https://vbn.aau.

[15] Poushpas, S. and Leithead, W.: Wind farm control through dynamic coordination of wind turbines reference power, Lisbon, Portugal, in: 1st International Conference on Renewable Energies Offshore, 2014, Lisbon, https://doi.org/10.1201/b18973-101.

[16] Bossanyi, E.: Combining induction control and wake steering for wind farm energy and fatigue loads optimisation, IOP Publ., 1037, 032011, https://doi.org/10.1088/1742-6596/1037/3/032011, 2018.

[17] Shapiro, C. R., Bauweraerts, P., Meyers, J., Meneveau, C., and Gayme, D. F.: Model-based receding horizon control of wind farms for secondary frequency regulation, Wind Energy, 20, 1261–1275, https://doi.org/10.1002/we.2093, 2017.

[18] Shapiro, C. R., Gayme, D. F., and Meneveau, C.: Modelling yawed wind turbine wakes: a lifting line approach, J. Fluid Mech., 841, R1, https://doi.org/10.1017/jfm.2018.75, 2018.

[19] Kheirabadi, A. C. and Nagamune, R.: A low-fidelity dynamic wind farm model for simulating time-varying wind conditions and floating platform motion, Ocean Eng., 234, 109313, https://doi.org/10.1016/j.oceaneng.2021.109313, 2021.

[20] Gebraad, P. M. O. and van Wingerden, J. W.: A Control-Oriented Dynamic Model for Wakes in Wind Plants, J. Phys.: Conf. Ser., 524, 012186, https://doi.org/10.1088/1742-6596/524/1/012186, 2014.

[21] Vogel, H.: A better way to construct the sunflower head, Math. Biosci., 44, 179–189, https://doi.org/10.1016/0025-5564(79)90080-4, 1979.

[22] Glauert, H., A General Theory of the Autogyro, HM Stationery Office, 1926.

[23] H. Glauert. Airplane Propellers, chapter Aerodynamic Theory, pages 169–360. Springer Berlin Heidelberg, 1935. doi:10.1007/978-3-642-91487-4_3.

[24] J Jonkman, S Butterfield, W Musial, and G Scott. Definition of a 5-mw reference wind turbine for offshore system development. 2 2009. doi: 10.2172/947422. URL https://www.osti.gov/biblio/947422.

[25] Yujoo Kang, Sang Lee; Wake effect on floating offshore wind turbine fatigue load. Physics of Fluids 1 December 2024; 36 (12): 125176. https://doi.org/10.1063/5.0242835 .

[26] R Thedin et al 2024 J. Phys.: Conf. Ser. 2767 032020, DOI 10.1088/1742-6596/2767/3/032020.